

A Statistical Framework for Understanding Causal Effects that Vary by Treatment Initiation Time in EHR-based Studies

Luke Benz¹, Rajarshi Mukherjee¹, Rui Wang^{1,2,3}, David Arterburn⁴, Heidi Fischer⁵, Catherine Lee⁶, Susan M. Shortreed^{7,8}, Alexander W. Levis^{*9}, and Sebastien Haneuse^{*1}

¹Department of Biostatistics, Harvard T.H. Chan School of Public Health, Boston, MA, USA

²Department of Population Medicine, Harvard Pilgrim Health Care Institute, Boston, MA, USA

³Department of Population Medicine, Harvard Medical School, Boston, MA, USA

⁴Kaiser Permanente Washington Health Research Institute, Seattle, WA, USA

⁵Department of Research & Evaluation, Kaiser Permanente Southern California, Pasadena, CA, USA

⁶Department of Epidemiology and Biostatistics, University of California San Francisco, San Francisco, CA, USA

⁷Biostatistics Division, Kaiser Permanente Washington Health Research Institute, Seattle, WA, USA

⁸Department of Biostatistics, University of Washington School of Public Health, Seattle, WA, USA

⁹Department of Biostatistics, Epidemiology and Informatics, University of Pennsylvania, Philadelphia, PA, USA

December 23, 2025

Abstract

Comparative effectiveness studies using electronic health records (EHR) consider data from patients who could “enter” the study cohort at any point during an interval that spans many years in calendar time. Unlike treatments in tightly controlled trials, real-world treatments can evolve over calendar time, especially if comparators include standard of care, or procedures where techniques may improve. Efforts to assess whether treatment efficacy itself is changing are complicated by changing patient populations, with potential covariate shift in key effect modifiers. In this work, we propose a statistical framework to estimate calendar-time specific average treatment effects and describe both how and why effects vary across treatment initiation time in EHR-based studies. Our approach projects doubly robust, time-specific treatment effect estimates onto candidate marginal structural models and uses a model selection procedure to best describe how effects vary by treatment initiation time. We further introduce a novel summary metric, based on standardization analysis, to quantify the role of covariate shift in explaining observed effect changes and disentangle changes in treatment effects from changes in the patient population receiving treatment. Extensive simulations using EHR data from Kaiser Permanente are used to validate the utility of the framework, which we apply to study changes in relative weight loss following two bariatric surgical interventions versus no surgery among patients with severe obesity between 2005–2011.

* denotes co-last author (AWL and SH)

Corresponding Author: Luke Benz (lukebenz@g.harvard.edu)

1 Introduction

Electronic health record (EHR) databases provide a useful data source for comparative effectiveness studies, allowing for larger sample sizes from patient populations which are more diverse than those typical of clinical trials (Casey et al., 2016). In EHR-based studies, study entry periods frequently extend over a decade or more (Arterburn et al., 2020, Coleman et al., 2016, Fisher et al., 2018, Haneuse et al., 2025, Harrington et al., 2024, O'Brien et al., 2013), perhaps because (a) treatment initiation is uncommon, (b) long-term outcomes are of interest, and/or (c) extending data collection further back in time requires little additional effort. For example, in a large EHR-based study, Arterburn et al. (2020) examined long-term weight loss outcomes of patients undergoing bariatric surgery between 2005-2015 in comparison to matched non-surgical controls. In contrast to treatment protocols in tightly controlled randomized clinical trials, real-world treatments, such as those examined by Arterburn et al. (2020), can evolve over time, especially if comparators include a somewhat loosely defined standard of care (Laiterapong and Huang, 2015) (e.g., for obesity management), or bariatric surgical procedures where techniques or best practices may change (Faria, 2017, Felsenreich et al., 2021, Guldogan et al., 2020, Sheetz et al., 2020). As such, causal effects of interest in EHR-based studies with long study entry periods may vary over the course of treatment initiation time, which we also refer to as calendar time throughout.

Heterogeneity in treatment initiation time has been discussed previously in the context of studies in pharmacoepidemiology. Common across such studies, however, is that variation in treatment initiation time is most often viewed as a potential source of bias towards estimating an implicitly assumed *constant* treatment effect across calendar time (though for longitudinal or time-to-event outcomes, the effect may vary across time since initiation). For example, stratification of propensity score models by calendar year has been suggested as a solution to address changes in physician prescription patterns or characteristics of treated patients over time (Dilokthornsakul et al., 2014, Dusetzina et al., 2013, Mack et al., 2013). When comparisons of interest involve, say, two drugs approved at different points in time, analysis is often restricted to a period where both medications are available to reduce differences attributable to calendar time (Gagne et al., 2013, Suissa et al., 2017). Strategies based on instrumental variables (Gokhale et al., 2018) and matching (Helin-Salmivaara et al., 2014) have also been proposed. In all, the predominant viewpoint has been that

variation in causal contrasts by calendar time is something that must be adjusted for, rather than adoption of causal estimands which explicitly use calendar time in their definition. That this is the case likely owes to the fact that in pharmacoepidemiologic studies, typical treatments (e.g., drugs or medications) are not changing over time. In such cases, there may be strong reason to believe there exists a common effect over calendar time in a static population, though the underlying populations may be shifting.

Causal estimands which depend on calendar time have recently been explored in the context of stepped-wedge cluster randomized trials (Lee et al., 2025, Wang et al., 2024) and staggered-adoption difference-in-difference settings (Callaway and Sant’Anna, 2021, Sun and Abraham, 2021), the latter of which often considers analysis of multi-year periods during which a policy is rolled out. Because intervention timing is planned or quasi-experimental across clusters, both study designs provide a natural way to define calendar time-specific effects for groups of clusters initiating treatment at the same time. By contrast, EHR-based studies analyze patient-level outcomes under naturally occurring treatment patterns, which do not follow any controlled schedule, and thus strategies from these literatures do not directly apply.

Determining whether causal effects vary over calendar time in EHR-based studies can help inform whether some fundamental aspect of treatment efficacy is changing, and whether researchers might report common or calendar time-varying effect estimates. However, efforts to assess whether treatment efficacy itself is changing are complicated by changing patient populations, and thus, potentially, covariate shift in key effect modifiers. As such, it is equally important to understand why causal effect estimates may vary over time, and the degree to which effect modification plays a role.

In this work, we propose a statistical framework to estimate and describe how and why causal effects vary over calendar time in EHR-based studies. First, doubly-robust, calendar time-specific average treatment effects (ATE) are estimated on the basis of pooled nonparametric nuisance models. Second, estimates are projected onto candidate marginal structural models (MSM), each representing a different pattern in how effect estimates vary across treatment initiation time (e.g., constant, linear etc.). A model selection procedure is then applied to choose which MSM best describes temporal variation in effect estimates. Next, we define a causal estimand that corresponds to the treatment effect that would arise if the distribution of covariates among eligible patients treated at a given point in time instead reflected the distribution observed at some alternative point in time. Finally,

we introduce a novel summary metric to quantify the role of covariate shift in explaining observed effect changes and disentangle changes in treatment effects from changes in the patient population receiving treatment. To our knowledge, this work is the first to apply tools from semiparametric theory (Kennedy, 2023, Tsiatis, 2006) to study calendar time-varying treatment effects in EHR-based studies.

This work is motivated by the use of EHR data to study weight loss outcomes following bariatric surgery, particularly in comparison to similarly obese patients who do not undergo surgery, a setting which is described in detail in Section 2, and woven throughout the work. Section 3 formalizes notation and describes calendar time-specific causal estimands. Sections 4 and 5 introduce statistical tools, based on semiparametric efficiency theory, for determining how and why causal effects vary over calendar time, respectively, while Section 6 outlines how analysts can synthesize information from estimation and inferential procedures outlined in previous sections to determine what to report in their own study. Section 7 returns to the motivating study to apply the methods outlined in this work, and finally, Section 8 concludes with discussion. Detailed proofs and simulations which validate tools from this framework are provided in the Supplementary Material.

2 An EHR-based Study of Bariatric Surgery

Bariatric surgery is an intervention to mitigate obesity and related comorbidities, with typical candidates having a body mass index (BMI) exceeding 35 kg/m^2 (Kaiser Permanente, 2023). Due to the cost and complexity of conducting large-scale trials for bariatric surgery (Courcoulas et al., 2024), EHR-based studies are a critical tool to study long-term outcomes following bariatric surgery, particularly in relation to similarly obese patients not undergoing surgery (Arterburn et al., 2020, Coleman et al., 2022, Fisher et al., 2018, Harrington et al., 2024, O’Brien et al., 2018). Despite its success as a weight-loss intervention, only 1-2% of eligible candidates elect to undergo bariatric surgery annually (Arterburn and Courcoulas, 2014). Therefore, EHR-based studies of bariatric surgery must consider a multi-year study entry period to obtain a meaningful number of patients undergoing surgery.

The two most common bariatric surgical procedures are Roux-en-Y gastric bypass (RYGB) and sleeve gastrectomy (SG), with SG having surpassed RYGB in frequency in the past 15 years (Arterburn and Courcoulas, 2014, Reames et al., 2014). SG is a less invasive and technically easier

procedure than RYGB, and as such is offered by more surgeons. Relevant to this work is that the surgical technique for SG has historically been somewhat less standardized than for RYGB, particularly during the time-frame during which SG became the more commonly performed procedure (Gagner et al., 2013, Guldogan et al., 2020, Rosenthal et al., 2012). Given the rapid shifts in the relative popularity of RYGB and SG in recent years, along with possibly evolving surgical techniques and standards of care for obesity management, understanding potential temporal changes in the effectiveness bariatric surgery is of particular interest.

With this backdrop, we examined relative weight change at four pre-specified times post-surgery (6 months, 1 year, 2 years, 3 years), comparing 17,905 patients undergoing bariatric surgery between 2005-2011 at one of three Kaiser Permanente (KP) sites (KP Washington, KP Northern California, KP Southern California) with 933,044 non-surgical patients. In particular, we compared outcomes between surgery and no surgery, each of RYGB/SG versus no surgery separately, and RYGB versus SG. We leveraged EHR data from DURABLE, an NIH-funded study examining long-term outcomes of bariatric surgery across Kaiser Permanente sites (Arterburn et al., 2020, Coleman et al., 2022, 2016, Fisher et al., 2018, Haneuse et al., 2025, Harrington et al., 2024, O'Brien et al., 2018).

Using this data source, Arterburn et al. (2020) previously characterized longitudinal weight trajectories following RYGB and SG in comparison to matched non-surgical patients, though calendar time was considered only as a potential confounder. As an alternative to the matched cohort design employed by Arterburn et al. (2020), we used a sequential target trial emulation approach (Benz et al., 2024, Cain et al., 2010, Caniglia et al., 2023, Danaei et al., 2013, Haneuse et al., 2025, Madenci et al., 2024). Specifically, we considered a sequence of 84 target trials (formalized in Section 3), initiating at monthly intervals between January 2005 and December 2011. Following Arterburn et al. (2020), our study population included adults aged 19-79 years with BMI 35 kg/m^2 . We excluded patients without a year of continuous enrollment in KP insurance and those pregnant in the year prior to the start of a particular target trial. 17,596 surgical patients (98.2%) and 763,016 non-surgical patients (81.8%) met the study inclusion criteria at baseline of at least one target trial.

On the basis of these data, one might choose to estimate and report common a effect for bariatric surgery on 3 year relative weight change, in comparison to non-surgical patients. Though formal details are deferred until Section 7, such an approach produced estimates of -19.8% (-19.9%, -19.6%) for surgery overall, with corresponding estimates of -23.1% (-23.3%, -22.9%) for RYGB and -16.3%

Distribution of Key Covariates in Study Population
Eligible Patients Undergoing Bariatric Surgery

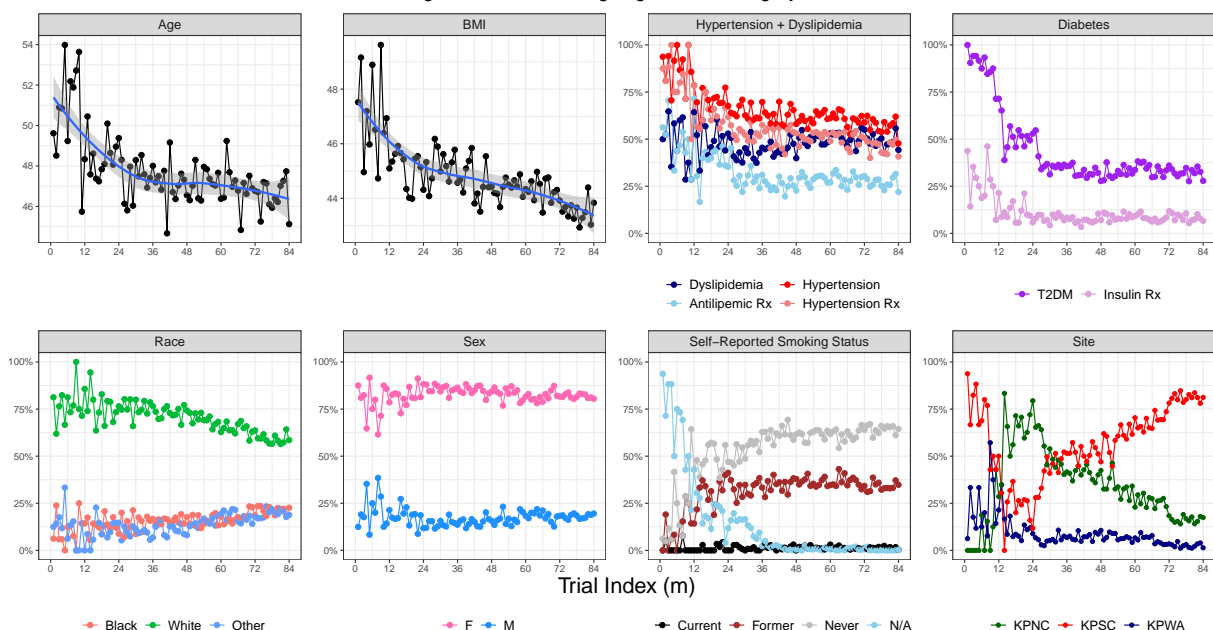


Figure 1: Distribution of patient characteristics in DURABLE electronic health record database over calendar time for eligible patients undergoing bariatric surgery between 2005-2011. Covariate mean values (continuous covariates) or frequency (binary/categorical covariates) are plotted by month of surgery. $m = 1$ corresponds to January 2005 and $m = 84$ corresponds to December 2011.

(-16.6%, -16.1%) and SG, in close agreement with estimates of -23.5% and -16.7% reported by Arterburn et al. (2020), respectively. These summaries, however, do not acknowledge the potential for variation across calendar time, and thus do not offer any insight into possible temporal variation in the effectiveness of bariatric surgery.

Figure 1 summarizes the distribution of several key covariates among eligible bariatric patients across the 84 target trials (i.e., across calendar time). Notably, the distribution of several effect modifiers highlighted by Arterburn et al. (2020) (age, BMI, race, and diabetes status) varies meaningfully across time of surgery. For example, the mean BMI of patients undergoing bariatric surgery in a given calendar month declines from 47.5 kg/m² in January 2005 to 43.8 kg/m² in December 2011, with monthly averages ranging between 42.9 kg/m² and 49.6 kg/m². Accordingly, any attempt to study how the effect of bariatric surgery may have changed over the course of the study period should acknowledge and account for this covariate shift. A similar figure displaying covariate shift for non-surgical patients is available in the Supplementary Materials (Figure S1).

3 Problem Setting

3.1 Notation

When a treatment strategy does not correspond to a concrete clinical event, time zero can be challenging to define (Hernán et al., 2016). In order to ensure that the start of follow-up is well-defined for all patients, particularly those not undergoing surgery, we partition the study entry period into a sequence of M target trials (Benz et al., 2024, Cain et al., 2010, Caniglia et al., 2023, Danaei et al., 2013, Madenci et al., 2024), indexed by $m \in \{1, \dots, M\}$. In the motivating study of bariatric surgery, $M = 84$ and component target trials are conducted at monthly intervals between January 2005 ($m = 1$) and December 2011 ($m = M = 84$).

To the best of our knowledge, the sequential target trial emulation design has been applied exclusively in applications examining time-to-event outcomes (Scola et al., 2023). Since relative weight change is not a time-to-event endpoint, we describe notation to formalize this design for continuous outcomes. Let $A_m \in \{0, 1\}$ denote a binary treatment (e.g., surgery vs. no surgery) received at baseline of trial m , $Y_m \in \mathbb{R}$ denote an outcome of interest (e.g., relative weight change since baseline of trial m), and $\mathbf{L}_m \in \mathbb{R}^p$ denote a set of covariates at baseline of trial m assumed sufficient for control of confounding, such as those in Figure 1. Let $E_m = g(\mathbf{L}_m)$ be a binary eligibility indicator for inclusion in target trial m , where $g(\cdot)$ represents a fixed and known eligibility rule (Benz et al., 2024, 2025). Practically, because not all patients are in the EHR for the entire duration of the study entry period, we treat subjects as ineligible ($E_m = 0$) for periods before they appear and/or after they disappear from the EHR. Thus, at each of M regularly occurring intervals, we ascertain (\mathbf{L}_m, A_m, Y_m) for eligible subject-trials; formally, we work with coarsened observed data units:

$$O = (E_1, E_1 \mathbf{L}_1, E_1 A_1, E_1 Y_1, \dots, E_m, E_m \mathbf{L}_m, E_m A_m, E_m Y_m, \dots, E_M, E_M \mathbf{L}_M, E_M A_M, E_M Y_M).$$

We observe a sample (O_1, \dots, O_n) of n independent and identically distributed observations from an underlying and unknown data distribution, P , i.e., the joint distribution of information across both patients and trials. Implicitly throughout, we assume covariates across trials share a common

domain \mathcal{L} . As will become apparent in Sections 3.2 and 4, covariate, treatment and outcome values of ineligible patients are not required for the definition of our calendar time-specific causal estimands, nor for estimation.

For any P -integrable function f we define $Pf = \mathbb{E}_P[f] = \int f dP$ to denote the expectation of f under P , and analogously define $\mathbb{P}_n f = \frac{1}{n} \sum_{i=1}^n f(O_i)$ to express the sample mean of f on data units (O_1, \dots, O_n) . Lastly, we let $Y_m(a_m)$ denote counterfactual outcomes at time m , that is the outcome that would have been observed under treatment $A_m = a_m$ (Hernán and Robins, 2024).

3.2 Calendar Time-Specific Average Treatment Effects

Towards understanding how and why treatment efficacy may vary over treatment initiation time, we define the following causal estimand:

$$\chi_m(P) = \mathbb{E}[Y_m(1) - Y_m(0) \mid E_m = 1].$$

Notice that $\chi_m(P)$ is simply the calendar time-specific ATE among patients eligible for trial m . Implicit in the definition of $\chi_m(P)$ is that comparisons are being made between the specific versions of treatment (i.e., surgical technique, standard of care) in place at time m . Note, $\chi_m(P)$ is an intention-to-treat (ITT) effect (Hernán and Robins, 2016) in the sense that it captures the effect of initiating treatment at time m ($a_m = 1$) versus not initiating ($a_m = 0$) without regard to what happens at future time points. In particular, the definition of $\chi_m(P)$ is not concerned that treatment definitions may evolve over time (e.g., $a_j = 0$ and $a_m = 0$ may mean slightly different things for $j > m$), nor for the possibility of treatment switching.

4 Estimation of Calendar Time-Specific Average Treatment Effects

Given that treatment decisions in EHR-based settings are not randomized, we begin by articulating standard causal inference assumptions to address the potential for confounding. Note that these assumptions are only required to hold among the subset of patients eligible for each trial. This is particularly salient for comparisons of bariatric surgery to no surgery, where study eligibility criteria are often designed to exclude patients who are not realistic candidates for surgery.

A1 (Consistency) $Y_m(A_m) = Y_m$ when $E_m = 1$, for all m .

A2 (Positivity) $\exists \epsilon > 0$ such that $\epsilon \leq P(A_m = 1 \mid \mathbf{L}_m, E_m = 1) \leq 1 - \epsilon$, almost surely, for all m .

A3 (No Unmeasured Confounding) $Y_m(a_m) \perp\!\!\!\perp A_m \mid \mathbf{L}_m, E_m = 1$ for $a_m \in \{0, 1\}$ and all m .

In our data application, we take \mathbf{L}_m to be the most recent values of covariates outlined in Figure 1, although we note that analysts can also include in this vector appropriate summaries of covariate and/or treatment history prior to baseline of trial m , if warranted in their application.

4.1 Motivating A Projection Parameter Approach

At the outset, estimation of each calendar time-specific ATE $\chi_m(P)$ may seem straightforward. Let $\mu_m(a_m, \mathbf{L}_m) = \mathbb{E}[Y_m \mid A_m = a_m, \mathbf{L}_m, E_m = 1]$ and $\pi_m(\mathbf{L}_m) = P(A_m = 1 \mid \mathbf{L}_m, E_m = 1)$ denote the trial m specific outcome regression and propensity score models, respectively. Under Assumptions 1-3, $\chi_m(P)$ is identified by the g -formula, $\mathbb{E}[\mu_m(1, \mathbf{L}_m) - \mu_m(0, \mathbf{L}_m) \mid E_m = 1]$ or via inverse probability weighting, $\mathbb{E}\left[\left(\frac{A_m}{\pi_m(\mathbf{L}_m)} - \frac{1-A_m}{1-\pi_m(\mathbf{L}_m)}\right)Y_m \mid E_m = 1\right]$ (Hernán and Robins, 2024). One might then proceed to estimate $\chi_m(P)$ on the basis of its nonparametric influence function (Kennedy, 2023, Tsiatis, 2006),

$$\begin{aligned} \dot{\chi}_m^*(O; P) = \frac{\mathbb{1}(E_m = 1)}{P(E_m = 1)} & \left\{ \mu_m(1, \mathbf{L}_m) - \mu_m(0, \mathbf{L}_m) - \chi_m(P) \right. \\ & \left. + \left(\frac{A_m}{\pi_m(\mathbf{L}_m)} - \frac{1-A_m}{1-\pi_m(\mathbf{L}_m)} \right) (Y_m - \mu_m(A_m, \mathbf{L}_m)) \right\}. \end{aligned}$$

Unfortunately, estimating μ_m or π_m by fitting a separate model for each trial would be difficult in practice, especially in settings where a relatively small number of patients initiate a particular treatment during trial m . For example, 24 of 84 target trials in our study have fewer than 100 patients undergoing bariatric surgery at the corresponding baseline month, and 12 of 84 of have fewer than 25 surgical patients. This problem is further compounded for comparisons involving the individual surgical procedures, RYGB and SG (Figure S2).

The predominant analytic strategy in sequential target trial emulations for time-to-event outcomes involves fitting a single parametric outcome and/or propensity score model pooling information across trials (Scola et al., 2023) (e.g., pooled logistic regression (D’Agostino et al., 1990)), perhaps with a spline term to flexibly adjust for calendar time as a confounder (Dickerman et al.,

2019, Madenci et al., 2024). Given that trends in $\chi_m(P)$ over calendar time may reflect a complex interplay between changing treatment efficacy and shifts in effect modifier distributions, applying a pooled parametric model in this setting would require correctly specifying a substantial number of flexible interactions between treatment, confounders, and calendar time. Such a task may be unrealistic in many instances—arguably including our data application given the heterogeneity reported in Figure 1—and might instead motivate the use of pooled models based on flexible machine learning methods.

Ultimately, while we are interested in trial-specific ATEs, we are most interested in the underlying trend in $\chi_m(P)$ across calendar time. To formalize estimation of this trend across calendar time, we follow the strategy of Kennedy et al. (2019) and others (Kennedy et al., 2023, Neugebauer and Van der Laan, 2007, Rosenblum and Van der Laan, 2010), and formulate our estimand as a projection of all M trial-specific effects onto a candidate parametric model. To operationalize this approach, we first define a MSM for mean trial-specific counterfactual outcomes.

$$\mathbb{E}[Y_m(a_m) \mid E_m = 1] = \psi_0(m) + \psi(m)a_m. \quad (1)$$

When the MSM in Equation (1) is saturated, $\psi(m) = \chi_m(P)$. Instead, we adopt a parametric model for $\psi(m)$, denoted $\psi(m; \boldsymbol{\beta})$, and take our estimand to be the projection of $\chi_m(P)$ onto $\psi(m; \boldsymbol{\beta})$. Formally, $\boldsymbol{\beta}(P)$ is the projection parameter defined by

$$\boldsymbol{\beta}(P) = \operatorname{argmin}_{\boldsymbol{\beta} \in \mathbb{R}^k} \sum_{m=1}^M h(m) \left(\chi_m(P) - \psi(m; \boldsymbol{\beta}) \right)^2,$$

where $h(m)$ is an optional trial-specific weight. Henceforth, we proceed with weights of the form $h(m) = w(m)P(E_m = 1)$ to weight trial contributions according to their effective sample size, where $w(m)$ allows for optional weighting by other additional factors.

This approach offers several advantages, which we elaborate on in subsequent sections. As will become clear in Section 4.2, estimation of $\chi_m(P)$ is a necessary step towards estimating $\psi(m; \boldsymbol{\beta})$, a task for which we advocate the use of pooled nuisance models based on flexible machine learning methods. Nevertheless, our projection parameter approach allows us to identify meaningful underlying trends in $\chi_m(P)$ even if some trial-specific effects are estimated imprecisely (e.g., due to small sample sizes). Although pooled nonparametric models for component nuisance functions will be an

essential step in estimating $\chi_m(P)$, they provide limited insight into how information is shared across calendar time. Introducing the additional projection step makes this information sharing explicit and clarifies how effect estimates from individual trials are combined to learn trends over calendar time, thereby improving transparency relative to relying on pooled nonparametric models alone. Finally, this approach naturally supports a model selection procedure (described in Section 4.4) for comparing candidate MSMs to identify the functional form that best describes how treatment effects vary over calendar time, including the possibility of a single, constant effect.

4.2 Efficient Estimation of Projection Parameter

We now introduce preliminary efficiency theory for the projection parameters $\beta(P)$, which will motivate our proposed estimator. Since influence functions are by definition mean zero, it is helpful to work with uncentered versions, $\dot{\chi}_m(O; P) := \frac{\mathbb{1}(E_m=1)}{P(E_m=1)} \dot{\chi}_m^\dagger(O; P)$, which satisfy $\mathbb{E}_P[\dot{\chi}_m(O; P)] = \chi_m(P)$, where

$$\dot{\chi}_m^\dagger(O; P) := \mu_m(1, \mathbf{L}_m) - \mu_m(0, \mathbf{L}_m) + \left(\frac{A_m}{\pi_m(\mathbf{L}_m)} - \frac{1 - A_m}{1 - \pi_m(\mathbf{L}_m)} \right) \left(Y_m - \mu_m(A_m, \mathbf{L}_m) \right).$$

These quantities play an important role in the influence function of $\beta(P)$, as summarized in the following theorem.

Theorem 1 *Suppose that the candidate MSM, $\psi(m; \beta)$ is twice differentiable in β . Then, under Assumptions 1-3, $\beta(P)$ is identified as the solution to the estimating equation,*

$$0 = \sum_{m=1}^M w(m) P(E_m = 1) \nabla_{\beta} \psi(m; \beta) [\chi_m(P) - \psi(m; \beta)].$$

Furthermore, $\hat{\beta}^*(O; P)$, the influence function of $\beta(P)$ (up to proportionality), is given by

$$\hat{\beta}^*(O; P) \propto \dot{\beta}^\dagger(O; P) = \sum_{m=1}^M \mathbb{1}(E_m = 1) w(m) \nabla_{\beta} \psi(m; \beta)|_{\beta=\beta(P)} \left(\dot{\chi}_m^\dagger(O; P) - \psi(m; \beta(P)) \right). \quad (2)$$

There are several observations from Theorem 1 worth pointing out. First, Equation (2) motivates an estimator $\hat{\beta}$ which solves $\mathbb{P}_n[\dot{\beta}^\dagger(O; \hat{P})] = 0$, that is,

$$0 = \sum_{m=1}^M w(m) \mathbb{P}_n(E_m = 1) \nabla_{\beta} \psi(m; \beta) |_{\beta=\hat{\beta}} \left\{ \hat{\chi}_m - \psi(m; \hat{\beta}) \right\}, \quad (3)$$

where $\hat{\chi}_m$ is the influence function-based estimator of $\chi_m(P)$ mentioned in Section 4.1, and \hat{P} indicates that any necessary nuisance functions are replaced by estimated quantities. Equations (2) and (3) make clear, however, that to even estimate $\beta(P)$, estimates of $\chi_m(P)$, and thus estimates of nuisance functions μ_m and π_m , are required. Also of note in Equation (3), trials are weighted proportionally to the sample size of their eligible populations, potentially mitigating the influence of noisier estimates of $\chi_m(P)$ in component trials with smaller sample sizes.

A subtle but important point is that the projection-based estimate of the treatment effect trend, $\psi(m; \hat{\beta})$, will reflect patterns in our estimates of $\chi_m(P)$, and thus, projections based on estimates $\hat{\chi}_m$ from pooled parametric models will mirror any structure implied by the adopted models. As such, it is necessary to maintain a sufficient degree of flexibility in estimating $\chi_m(P)$ and only adopt any structure (e.g., to characterize the underlying trend) after trial-specific ATEs have been estimated. We revisit the topic of selecting how much structure to adopt on top of $\hat{\chi}_m$ in Section 4.4.

In order to estimate $\chi_m(P)$, we first create a pooled dataset \mathcal{D} of patient information across all trials in which they are eligible, that is,

$$\mathcal{D} = \bigcup_{m=1}^M \left\{ (\mathbf{L}_{m,i}, A_{m,i}, Y_{m,i}, m) \right\}_{i:E_{m,i}=1}. \quad (4)$$

We then use \mathcal{D} to estimate a pooled outcome regression $\tilde{\mu}(A_m, \mathbf{L}_m, m)$ and propensity score model $\tilde{\pi}(\mathbf{L}_m, m)$. Notice that the trial index, m , is included as a covariate in the estimation of these pooled models. Not only does this ensure that fitted nuisance functions $\hat{\mu}_m(A_m, \mathbf{L}_m) \equiv \tilde{\mu}(A_m, \mathbf{L}_m, m)$ and $\hat{\pi}_m(\mathbf{L}_m) \equiv \tilde{\pi}(\mathbf{L}_m, m)$ maintain a dependence on calendar time, but also when flexible modeling strategies are employed, it allows the strength of association between covariates in \mathbf{L} and treatment or outcome to vary over calendar time as well. Given the potential for complex interactions between treatment, confounders, and calendar time, employing machine learning models which can handle complex interaction, such as random forests, is particularly important. In a similar vein, we recommend stratification of the outcome model by treatment status to allow for greater flexibility, that is estimating separate pooled models $\tilde{\mu}_1(\mathbf{L}_m, m)$ for $A_m = 1$ and $\tilde{\mu}_0(\mathbf{L}_m, m)$ for $A_m = 0$.

Using nuisance function estimates from pooled models, we then estimate $\chi_m(P)$ with the influence function-based estimator $\mathbb{P}_n \left[\frac{\mathbb{1}(E_m=1)}{\mathbb{P}_n[E_m]} \dot{\chi}_m^\dagger(O; \hat{P}) \right]$, i.e., which solves $\mathbb{P}_n[\dot{\chi}_m^*(O; \hat{P})] = 0$.

Routines for estimation of influence function-based estimators like $\hat{\chi}_m$ or $\hat{\beta}$ and typically involve sample splitting or cross-fitting, particularly when using nonparametric and/or machine learning techniques to estimate component nuisance functions (Chernozhukov et al., 2018). We describe the complete procedure for estimating $\hat{\chi}_m$ and $\hat{\beta}$ below.

Algorithm 1 (Computation of $\hat{\chi}_m$ and $\hat{\beta}$) *Let S_1 and S_2 be two disjoint, independent splits of (O_1, \dots, O_n) of sizes n_1 and n_2 , respectively, with $n = n_1 + n_2$. The analytical procedure to compute the estimator $\hat{\chi}_m$ and $\hat{\beta}$ is as follows:*

1. Create pooled dataset of eligible subject-trials \mathcal{D}_1 among the n_1 subjects in split S_1 , as in Equation (4).
2. Fit pooled models $(\tilde{\mu}_1, \tilde{\mu}_0, \tilde{\pi})$ on \mathcal{D}_1 to obtain nuisance estimators $\hat{P}_1 := \{(\hat{\mu}_m, \hat{\pi}_m)\}_{m=1}^M$.
3. For $O_{n_1+1}, O_{n_1+2}, \dots, O_n \in S_2$, construct plug-in estimates of uncentered influence functions $\{\dot{\chi}_m(O_i; \hat{P}_1)\}_{i=n_1+1}^n$ for each $m \in \{1, \dots, M\}$, where $\dot{\chi}_m(O_i; \hat{P}_1) \equiv \frac{\mathbb{1}(E_m=1)}{\mathbb{P}_n[E_m]} \dot{\chi}_m^\dagger(O_i; \hat{P}_1)$.
4. Repeat steps 1-3, swapping the roles of S_1 and S_2 to create, for each $m \in \{1, \dots, M\}$, complete sets of influence function contributions from corresponding out-of-sample nuisance function predictions, $\{\dot{\chi}_m(O_i; \hat{P})\}_{i=1}^n = \{\dot{\chi}_m(O_i; \hat{P}_1)\}_{i=n_1+1}^n \cup \{\dot{\chi}_m(O_i; \hat{P}_2)\}_{i=1}^{n_1}$.
5. Compute calendar time-specific treatment effects, $\hat{\chi}_m = n^{-1} \sum_{i=1}^n \dot{\chi}_m(O_i; \hat{P})$.
6. For a given candidate marginal structural model, $\psi(m; \beta)$, plug estimates $\{\hat{\chi}_m\}_{m=1}^M$ into Equation (3) and solve for $\hat{\beta}$ (e.g., via `nleqslv` (Hasselmann, 2023)).

4.3 Theoretical Properties of $\hat{\beta}$ and $\hat{\chi}_m$

The choice to estimate $\hat{\chi}_m$ and $\hat{\beta}$ using an estimating equation-based approach rather than a one-step approach is a matter of practical convenience; asymptotically the two approaches are equivalent. In order to describe the asymptotic behavior of $\hat{\beta}$, we note that $\text{Var}[\hat{\beta}^*(O; P)] = \mathbf{V}^{-1} \mathbf{C} \mathbf{V}^{-1}$, where $\mathbf{V} \in \mathbb{R}^{k \times k}$ is the scaling matrix of proportionality ignored in Theorem 1, and $\mathbf{C} = \text{Var}[\dot{\beta}^\dagger(O; P)] \in \mathbb{R}^{k \times k}$. As we derive in Supplementary Materials Appendix S1, we have that

$$\mathbf{V} = \sum_{m=1}^M w(m) P(E_m = 1) \left\{ \nabla_{\beta\beta}^2 \psi(m; \beta) |_{\beta=\beta(P)} [\chi_m(P) - \psi(m; \beta(P))] - \nabla_{\beta} \psi(m; \beta) |_{\beta=\beta(P)} [\nabla_{\beta} \psi(m; \beta) |_{\beta=\beta(P)}]^T \right\}. \quad (5)$$

Finally, we summarize the asymptotic behavior of $\widehat{\chi}_m$ and $\widehat{\beta}$ in the following theorem. Henceforth, we write $\|f\|_{(m)}$ for the $L_2(P)$ norm of a function of (\mathbf{L}_m, A_m, Y_m) conditional on eligibility in the m^{th} trial: $\|f\|_{(m)}^2 := \mathbb{E}_P[f(\mathbf{L}_m, A_m, Y_m)^2 | E_m = 1]$.

Theorem 2 *Suppose $\|\widehat{\pi}_m - \pi_m\|_{(m)} + \sum_{a=0}^1 \|\widehat{\mu}_m(a, \cdot) - \mu_m(a, \cdot)\|_{(m)} = o_P(1)$. Further, assume that $\epsilon \leq \widehat{\pi}_m(\mathbf{L}_m), \pi(\mathbf{L}_m) \leq 1 - \epsilon$ and $|Y_m|, |\widehat{\mu}_m(a, \mathbf{L}_m)| \leq \epsilon^{-1}$ almost surely when $E_m = 1$. Then*

$$\widehat{\chi}_m - \chi_m(P) = \mathbb{P}_n[\dot{\chi}_m^*(O; P)] + O_P(\widehat{R}_m) + o_P(n^{-1/2}),$$

where

$$\widehat{R}_m = \|\widehat{\pi}_m - \pi_m\|_{(m)} \sum_{a=0}^1 \|\widehat{\mu}_m(a, \cdot) - \mu_m(a, \cdot)\|_{(m)}.$$

Moreover, if $\widehat{R}_m = o_P(n^{-1/2})$ then $\sqrt{n}(\widehat{\chi}_m - \chi_m(P)) \xrightarrow{d} \mathcal{N}(0, \text{Var}[\dot{\chi}_m^*(O, P)])$, whereby $\widehat{\chi}_m$ attains the nonparametric efficiency bound.

Similarly, under Assumptions S1-S3 in Appendix S1.3,

$$\widehat{\beta} - \beta(P) = \mathbb{P}_n[\dot{\beta}^*(O; P)] + O_P\left(\sum_{m=1}^M \widehat{R}_m\right) + o_P(n^{-1/2}).$$

When $\sum_{m=1}^M \widehat{R}_m = o_P(n^{-1/2})$, $\sqrt{n}(\widehat{\beta} - \beta(P)) \xrightarrow{d} \mathcal{N}(0, \text{Var}[\dot{\beta}^*(O; P)])$, whereby $\widehat{\beta}$ attains the nonparametric efficiency bound.

As illustrated by Theorem 2, the rates of convergence for estimates of calendar time-specific treatment effects and their corresponding trend are directly tied to error rates in estimation of the underlying outcome regression and propensity score models. Importantly, convergence rates for both $\widehat{\chi}_m$ and $\widehat{\beta}$ are faster than component nuisance functions, even when employing flexible modeling choices. When these product errors are $o_P(n^{-1/2})$ —for example when each nuisance function’s error rate is $o_P(n^{-1/4})$ —then $\widehat{\chi}_m$ is \sqrt{n} -consistent and asymptotically normal, and attains the nonparametric efficiency bound. Furthermore, when the required rate conditions are satisfied for each component trial the same properties extend to $\widehat{\beta}$. Additional commentary on Assumptions S1-S3 is provided in the Supplementary Materials.

Pooled models can help ensure that the required rate conditions are met in component trials with smaller effective sample sizes. As discussed in Section 4.2, however, pooled parametric models

for π_m and μ_m are likely to be inconsistent in the presence of significant covariate shift, motivating the use of more flexible pooled models. Crucially, when the required rate conditions (e.g., $o_P(n^{-1/4})$ for each nuisance function) are satisfied, asymptotically valid inference for the trend in treatment effects across calendar time remains attainable, even when using such flexible pooled models.

In particular, asymptotically valid pointwise Wald-style $(1 - \alpha)$ -level confidence intervals are given by

$$\begin{aligned} & \psi(m; \hat{\boldsymbol{\beta}}) \pm z_{1-\alpha/2} \sqrt{\nabla_{\boldsymbol{\beta}} \psi(m; \boldsymbol{\beta})|_{\hat{\boldsymbol{\beta}}}^T \mathbb{P}_n[\dot{\boldsymbol{\beta}}^*(O, \hat{P})^2] \nabla_{\boldsymbol{\beta}} \psi(m; \boldsymbol{\beta})|_{\hat{\boldsymbol{\beta}}}/n} \\ & = \psi(m; \hat{\boldsymbol{\beta}}) \pm z_{1-\alpha/2} \sqrt{\nabla_{\boldsymbol{\beta}} \psi(m; \boldsymbol{\beta})|_{\hat{\boldsymbol{\beta}}}^T \hat{\mathbf{V}}^{-1} \hat{\mathbf{C}} \hat{\mathbf{V}}^{-1} \nabla_{\boldsymbol{\beta}} \psi(m; \boldsymbol{\beta})|_{\hat{\boldsymbol{\beta}}}/n}, \end{aligned}$$

where z_α denotes the α quantile of the standard normal distribution. In the above, $\hat{\mathbf{V}}$ denotes the result of Equation (5) replacing $\boldsymbol{\beta}(P)$ and $\chi_m(P)$ with $\hat{\boldsymbol{\beta}}$ and $\hat{\chi}_m$, respectively, while $\hat{\mathbf{C}} = \widehat{\text{Var}}[\boldsymbol{\beta}^\dagger(O; \hat{P})]$.

4.4 Model Selection Among Candidate Marginal Structural Models

Suppose one considers a range of candidate MSMs including a constant model (i.e., $\psi(m; \boldsymbol{\beta}) = \beta$), a linear model (i.e., $\psi(m; \boldsymbol{\beta}) = \beta_0 + \beta_1 m$), and more flexible MSMs including higher-order polynomials (in m) and splines. A model selection procedure to select the MSM which best describes the underlying trend $\chi_m(P)$ is important to best characterize *how* treatment effects—and thus possibly treatment efficacy—vary over calendar time. In particular, if a constant model were selected, it would suggest that any underlying variation in treatment effects is not detectable given the study sample size, and thus may not be clinically meaningful. On the other hand, if a flexible MSM were selected, it would provide evidence of non-constant trends in treatment effects over calendar time.

To implement such a model selection procedure, we adapt the ideas of [Kennedy et al. \(2019\)](#) and [van der Laan and Dudoit \(2003\)](#). Let $\{\hat{\psi}_1, \dots, \hat{\psi}_K\}$ denote a set of K candidate MSM projection models, with $\hat{\psi}_k \equiv \psi_k(m; \hat{\boldsymbol{\beta}}_k)$. A natural quantity by which to compare candidate MSMs is mean-squared error (relative to the true $\chi_m(P)$). To simplify comparisons, we drop terms that don't depend on the candidate MSM and proceed with the pseudorisk,

$$L(\hat{\psi}_k) = \sum_{m=1}^M w(m) \{ \psi_k(m; \hat{\boldsymbol{\beta}}_k)^2 - 2\psi_k(m; \hat{\boldsymbol{\beta}}_k) \chi_m(P) \}.$$

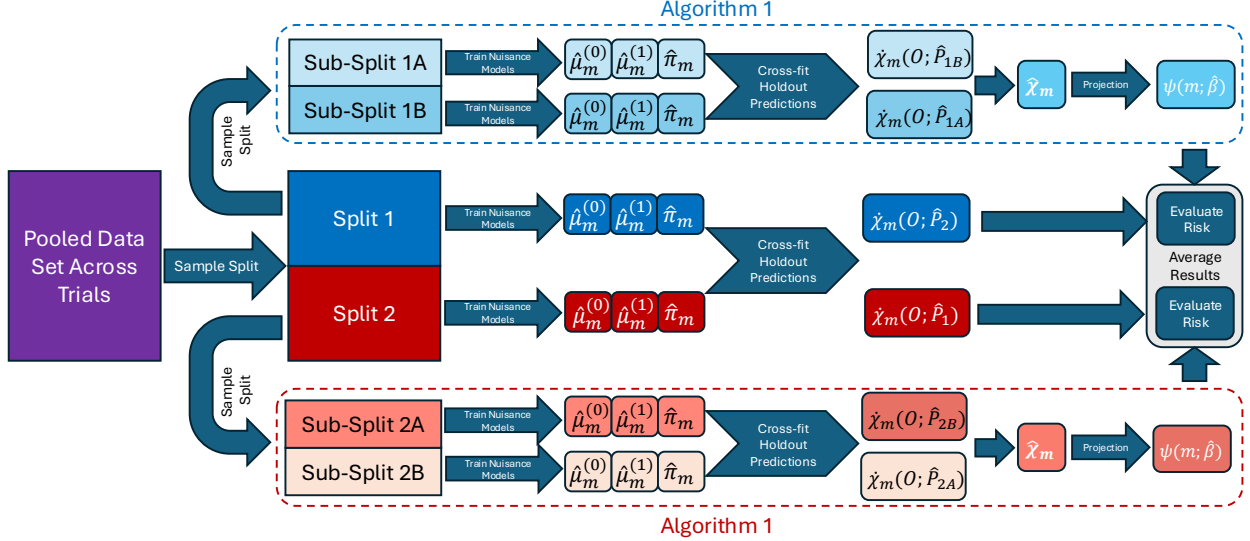


Figure 2: Overview of cross-fitting procedure for evaluating $\widehat{L}(\widehat{\psi}_k)$.

Given the appearance of $\chi_m(P)$ in the pseudorisk, we replace $\chi_m(P)$ with estimates based on its influence function, i.e., we proceed with the influence function-based estimator of the pseudorisk,

$$\widehat{L}(\widehat{\psi}_k) = \mathbb{P}_n \left[\sum_{m=1}^M w(m) \{ \psi_k(m; \widehat{\beta}_k)^2 - 2\psi_k(m; \widehat{\beta}_k) \dot{\chi}_m(O; \widehat{P}) \} \right].$$

This is an intuitive loss function to work with because it reflects an estimating equation-based estimator of the pseudorisk, based on its influence function, treating $\widehat{\psi}_k$ as fixed (Kennedy et al., 2019).

In contrast to loss functions like mean squared prediction error, which can be directly evaluated on holdout data via cross validation, careful evaluation of the pseudorisk requires that $\beta_k(P)$ and $\chi_m(P)$ are estimated on independent samples of data. However, we also require estimates of $\chi_m(P)$ in order to estimate the projection parameter $\beta_k(P)$. Thus, we proceed with a modified version of Algorithm 1, and introduce a second layer of sample splitting. Within each split of data at the first stage, we apply the entire Algorithm 1 to obtain our projection-based MSM on that split. Next we estimate $\dot{\chi}_m(O; \widehat{P})$ on the opposite data split by applying steps 1-3 of Algorithm 1, and combine results to compute $\widehat{L}(\widehat{\psi})$. Finally, we swap the roles of first-stage splits and average. This procedure is illustrated in Figure 2.

In practice, differences between candidate projection models can be small (Kennedy, 2023), particularly if models classes are nested within one another. In such cases, we might have a preference

for simpler models, such that more flexible MSMs are selected only if there are clinically meaningful trends in $\chi_m(P)$ across calendar time. To formalize this, let $\hat{\psi}^* = \operatorname{argmin}_{\hat{\psi}_k \in \{\hat{\psi}_1, \dots, \hat{\psi}_K\}} \widehat{L}(\hat{\psi}_k)$ denote the MSM among our set of candidates which minimizes the loss function $\widehat{L}(\hat{\psi}_k)$. Let

$$\epsilon = \sqrt{\frac{\sum_{m=1}^M w(m) \mathbb{P}_n(E_m = 1) \widehat{\operatorname{Var}}[\psi^*(m, \hat{\boldsymbol{\beta}})]}{\sum_{m=1}^M w(m) \mathbb{P}_n(E_m = 1)}}.$$

One can interpret ϵ as a pooled standard deviation across our best estimate of the calendar time trend, weighting proportional to the size of the eligible population at each trial. Finally, one can choose the simplest model such that $|\widehat{L}(\hat{\psi}_k) - \widehat{L}(\hat{\psi}^*)| \leq c\epsilon$, for some user-selected constant c . There is considerable debate in the literature about how large an effect size needs to be on a standard deviation scale to be clinically meaningful (Tsujiimoto et al., 2022), though the notion of clinically meaningful is very application dependent. In simulations, we find that $c = 1/4$ works well in our setup, but present result for a range of other values. Finally, we note that notion of “simpler model” can be operationalized through any model complexity criterion so long as models can be ordered by this criterion. One reasonable such choice—which we adopt in our application—is ordering candidate MSMs by the dimension of their indexing projection parameter (i.e., the dimension of $\boldsymbol{\beta}$).

5 Decomposing Sources of Variation

While the projection parameter framework and corresponding model selection procedure outlined in Section 4 provide insight into *how* treatment effects vary across calendar time, they fail to explain *why* such changes (if any) are observed. In particular, if the candidate MSM selected is non-constant, suggesting that $\chi_m(P)$ varies over time, we would like to ascertain the degree to which underlying changes in treatment efficacy—as opposed to distribution shift in effect modifiers—are responsible.

5.1 A Cross-Trial Contrast to Remove Distribution Shift

To isolate why treatment effects might vary over calendar time, we begin by defining new contrasts by reweighting mean counterfactual outcomes across eligible populations at different points in time:

$$\chi_{j,m}(P) := \int_{\mathcal{L}} \mathbb{E}[Y_m(a_m = 1) - Y_m(a_m = 0) \mid \mathbf{L}_m = \boldsymbol{\ell}, g(\mathbf{L}_m) = 1] dP_{\mathbf{L}_j | E_j = 1}(\boldsymbol{\ell} \mid E_j = 1).$$

The estimand $\chi_{j,m}(P)$ represents the difference in mean counterfactual outcomes at time m in a population where trial baseline covariates are standardized to the covariate distribution of the eligible population at time j . First, we note that when $j = m$, this contrast reduces to trial-specific ATE defined in Section 3.2, that is, $\chi_{m,m}(P) = \chi_m(P)$. Given the definition of the class of estimands $\chi_{j,m}(P)$, one obtains common populations with which to standardize treatment effects across calendar time. Namely, for $m_1 \neq m_2$, differences between $\chi_{j,m_1}(P)$ and $\chi_{j,m_2}(P)$ cannot be attributable to covariate shift, as the underlying population on which the causal contrast is defined is the same. We exploit this fact in Section 5.3 to introduce a metric for quantifying effect modification.

In order to identify each $\chi_{j,m}(P)$, we introduce an additional assumption similar to those commonly used in transportability analyses (Dahabreh et al., 2019, 2020, Ung et al., 2025).

A4 (Cross-Trial Overlap) For any $\ell \in \mathcal{L}$, $p(\ell \mid E_j = 1) > 0 \implies p(\ell \mid E_m = 1) > 0$.

Assumption 4 is often referred to as an overlap assumption in the transportability literature and ensures that if a patient met the study eligibility criteria at baseline of trial j , their covariate vector \mathbf{L}_j is in the support of the covariate distribution among those eligible for trial m .

Lemma 1 Under Assumptions 1-4, $\chi_{j,m}(P)$ is identified by

$$\chi_{j,m}(P) = \mathbb{E}[\mu_m(1, \mathbf{L}_j) - \mu_m(0, \mathbf{L}_j) \mid E_j = 1] = \int_{\mathcal{L}} \{\mu_m(1, \ell) - \mu_m(0, \ell)\} dP_{\mathbf{L}_j \mid E_j=1}(\ell).$$

5.2 Estimation of Cross-Trial Effects

Given that the cross-trial effects are just modified versions of calendar time-specific ATEs, the estimation strategy for $\chi_{j,m}(P)$ will be very similar to that of $\chi_m(P)$. We define one additional nuisance function, $\xi_{j,m}(\ell) = \frac{p(\mathbf{L}_j=\ell \mid E_j=1)}{p(\mathbf{L}_m=\ell \mid E_m=1)}$, which represents a density ratio to transport the covariate distribution of the eligible population in trial m to that of trial j .

Theorem 3 The influence function of $\chi_{j,m}$ at P in a nonparametric model is given by

$$\begin{aligned} \dot{\chi}_{j,m}^*(O; P) &= \frac{\mathbb{1}(E_j = 1)}{P(E_j = 1)} \{ \mu_m(1, \mathbf{L}_j) - \mu_m(0, \mathbf{L}_j) - \chi_{j,m}(P) \} \\ &\quad + \frac{\mathbb{1}(E_m = 1)}{P(E_m = 1)} \xi_{j,m}(\mathbf{L}_m) \left(\frac{A_m}{\pi_m(\mathbf{L}_m)} - \frac{1 - A_m}{1 - \pi_m(\mathbf{L}_m)} \right) (Y_m - \mu_m(A_m, \mathbf{L}_m)). \end{aligned}$$

The influence function $\dot{\chi}_{j,m}^*(O; P)$ admits a very intuitive form. The first summand resembles a g -formula estimating function using the outcome regression for trial m on the eligible covariate distribution from trial j . The second summand takes the inverse treatment-weighted residuals from eligible patients in trial m , and additionally weights them by the appropriate density ratio required to transport to trial j . If a subject is eligible for both trials j and m , they will contribute in both terms, increasing efficiency, but they can still contribute if eligible for only one of the trials.

Eventually, we will need to estimate $\chi_{j,m}(P)$ for all M^2 pairs of component target trials. As such, fitting a separate model for each $\xi_{j,m}$ is computationally infeasible. Moreover, conditional density estimation is a challenging statistical problem (Wasserman, 2006). Because $\xi_{j,m}$ is a ratio of conditional densities, however, we can directly apply Bayes' rule (Benz et al., 2025, Díaz et al., 2023, Sugiyama et al., 2012) and leverage pooled models, as with $\tilde{\mu}, \tilde{\pi}$:

$$\xi_{j,m}(\boldsymbol{\ell}) = \frac{p(\mathbf{L}_j = \boldsymbol{\ell} \mid E_j = 1)}{p(\mathbf{L}_m = \boldsymbol{\ell} \mid E_m = 1)} = \frac{P(E_m = 1)P(T = j \mid \mathbf{L} = \boldsymbol{\ell}, E = 1)}{P(E_j = 1)P(T = m \mid \mathbf{L} = \boldsymbol{\ell}, E = 1)}, \quad (6)$$

where T denotes the trial membership indicator in full the pooled data set, \mathcal{D} . Thus, we have turned the task of conditional density estimation into modeling the trial membership indicator conditional on \mathbf{L} across all eligible subject-trials. Crucially, this is a classification task well suited for machine learning methods, and we can apply any flexible pooled model $\tilde{\xi}(m \mid \boldsymbol{\ell})$ to estimate $P(T = m \mid \mathbf{L} = \boldsymbol{\ell}, E = 1)$.

With additional bookkeeping, we can estimate $\chi_{j,m}(P)$ for all pairs (j, m) within the same routine described by Algorithm 1. First, $\tilde{\xi}$ is trained during step 2 along with the other pooled models. Following step 3, for each row in \mathcal{D} , we save predicted transport ratios to all other trial populations, $\{\hat{\xi}_{j,m}(\mathbf{L}_m)\}_{j=1}^M$, and fitted values for the outcome regression at all possible treatment times, $\{(\hat{\mu}_m(1, \mathbf{L}_j), \hat{\mu}_m(0, \mathbf{L}_j))\}_{m=1}^M$. Extracting $\hat{\mu}_m(a_m, \mathbf{L}_j) = \tilde{\mu}(a_m, \mathbf{L}_j, m)$ simply requires (artificially) varying the trial index in the pooled model. Upon repeating these steps for both splits of (O_1, \dots, O_n) , we estimate each cross-trial effect via the following influence function-based estimator:

$$\hat{\chi}_{j,m} = \mathbb{P}_n \left[\frac{\mathbf{1}(E_j = 1)}{\mathbb{P}_n[E_j]} \{ \hat{\mu}_m(1, \mathbf{L}_j) - \hat{\mu}_m(0, \mathbf{L}_j) \} + \frac{\mathbf{1}(E_m = 1)}{\mathbb{P}_n[E_m]} \hat{\xi}_{j,m}(\mathbf{L}_m) \left(\frac{A_m}{\hat{\pi}_m(\mathbf{L}_m)} - \frac{1 - A_m}{1 - \hat{\pi}_m(\mathbf{L}_m)} \right) \left(Y_m - \hat{\mu}_m(A_m, \mathbf{L}_m) \right) \right],$$

where, recall, hatted quantities are estimated in the training split, and \mathbb{P}_n represents the empirical mean over the test split.

5.3 Summarizing Changes in Effect Estimates

Ultimately, our interest in $\chi_{j,m}(P)$ is as a stepping stone towards determining the degree to which changes in calendar time-specific treatment effects are explained by changes in effects modifiers compared to something more fundamental in terms of changes in underlying treatment efficacy. We let $\mathbf{S} \in \mathbb{R}^{M \times M}$ denote the standardization matrix of all M^2 cross-trial effects, with $S_{jm} = \chi_{j,m}(P)$, and let $\widehat{\mathbf{S}}$ denote the estimated standardization matrix with entries $\widehat{\chi}_{j,m}$. To quantify sources of variation in cross-trials effects, we define the following variance-like quantities:

$$\sigma_j^2 := \frac{1}{M-1} \sum_{m=1}^M \left(\chi_j(P) - \chi_{j,m}(P) \right)^2,$$

$$\gamma_m^2 := \frac{1}{M-1} \sum_{j=1}^M \left(\chi_m(P) - \chi_{j,m}(P) \right)^2.$$

Note that these quantities correspond to the row-wise and column-wise variances of \mathbf{S} , respectively. The quantity σ_j^2 characterizes the variability around the trial-specific ATE that would arise if the eligible population at time j had been treated at alternative time points. In contrast, γ_m^2 characterizes the variability around $\chi_m(P)$ across all trial-eligible populations, had each been treated at time m . To quantify the degree to which trends across calendar time might be attributable to covariate shift, we examine the ratio

$$\theta = \frac{1}{M} \sum_{m=1}^M \theta_m = \frac{1}{M} \sum_{m=1}^M \frac{\sigma_m^2}{\sigma_m^2 + \gamma_m^2}.$$

Using our estimated cross-trial effects, $\widehat{\chi}_{j,m}$, we can readily obtain plug-in estimates $\widehat{\sigma}_m^2$ and $\widehat{\gamma}_m^2$, and subsequently $\widehat{\theta}$, which offers a useful way to summarize variation across estimated cross-trial effects: $\widehat{\theta}$ can be interpreted as the average proportion of variation in estimated cross-trial effects attributable to factors other than covariate shift, e.g., changes in treatment efficacy. Conditions under which alternatives to changes in treatment efficacy may contribute to variation in cross-trial effects are discussed in greater detail in Section 6.

When $\theta = 0$, all $\sigma_m^2 = 0$, meaning that within fixed populations, there is no variation in treatment

effects across calendar time. In the event that a non-constant candidate MSM is selected, $\theta = 0$ indicates that the trend across treatment initiation time is entirely induced by changes in underlying populations. On the other hand, when $\theta = 1$, all $\gamma_m^2 = 0$, and thus variation in cross-trial effects is fully explained by changing the calendar time index (m). Importantly, $\theta = 1$ implies that trends across calendar time are not the result of covariate shift. Finally, when $\theta \in (0, 1)$, variation in estimated cross-trial effects is partially, but not entirely explained by distribution shift in effect modifiers. Formal hypothesis testing using θ is discussed in Section 5.5. Complete discussion of using θ , along with $\psi(m; \beta)$ from Section 4, to explain both *how* and *why* causal effects may vary over calendar time, is presented in Section 6.

5.4 Theoretical Properties of $\widehat{\chi}_{j,m}$

We briefly summarize the asymptotic behavior of $\widehat{\chi}_{j,m}$, which will be necessary for inference on θ .

Theorem 4 *Suppose $\|\widehat{\xi}_{j,m} - \xi_{j,m}\|_{(m)} + \|\widehat{\pi}_m - \pi_m\|_{(m)} + \sum_{a=0}^1 \|\widehat{\mu}_m(a, \cdot) - \mu_m(a, \cdot)\|_{(m)} = o_P(1)$. Further, assume that $\epsilon \leq \widehat{\pi}_m(\mathbf{L}_m), \pi(\mathbf{L}_m) \leq 1 - \epsilon$ and $|Y_m|, |\widehat{\mu}_m(a, \mathbf{L}_m)|, |\xi_{j,m}|, |\widehat{\xi}_{j,m}| \leq \epsilon^{-1}$ almost surely when $E_m = 1$. Then*

$$\widehat{\chi}_{j,m} - \chi_{j,m}(P) = \mathbb{P}_n[\widehat{\chi}_{j,m}^*(O; P)] + O_P(\widehat{R}_{j,m}) + o_P(n^{-1/2}),$$

where

$$\widehat{R}_{j,m} = \sum_{a=0}^1 \|\widehat{\mu}_m(a, \cdot) - \mu_m(a, \cdot)\|_{(m)} \left\{ \|\widehat{\xi}_{j,m} - \xi_{j,m}\|_{(m)} + \|\widehat{\pi}_m - \pi_m\|_{(m)} \right\}.$$

Moreover, if $\widehat{R}_{j,m} = o_P(n^{-1/2})$ then $\sqrt{n}(\widehat{\chi}_{j,m} - \chi_{j,m}(P)) \xrightarrow{d} \mathcal{N}(0, \text{Var}[\widehat{\chi}_{j,m}^*(O, P)])$, whereby $\widehat{\chi}_{j,m}$ attains the nonparametric efficiency bound.

The asymptotic behavior of $\widehat{\chi}_{j,m}$ is very similar to that of $\widehat{\chi}_m$, with an additional requirement that the product error between transport model $\xi_{j,m}$ and outcome model μ_m is $o_P(n^{-1/2})$. This rate condition is not unreasonable in light of Equation (6), and the choice to model trial index probabilities rather than conditional densities directly. We will leverage the asymptotic normality of $\widehat{\chi}_{j,m}$ in the following section when conducting inference for θ .

5.5 Hypothesis Testing for θ

Consider the hypothesis test $H_0 : \theta \in \{0, 1\}$ versus $H_1 : \theta \in (0, 1)$. We frame the null hypothesis as simultaneously testing two point nulls because $\theta = 0$ and $\theta = 1$ correspond to the cases where all or none of the variation in cross-trial effects, respectively, is explained by changes in underlying populations, respectively. Rejection of H_0 for this test is equivalent to simultaneous rejection of the two one-sided tests, $H_0^{(0)} : \theta = 0$ versus $H_1^{(0)} : \theta > 0$ and $H_0^{(1)} : \theta = 1$ versus $H_1^{(1)} : \theta < 1$. Drivers of treatment effect heterogeneity across calendar time differ based on whether $\theta = 1$ or $\theta \in (0, 1)$, and thus only testing the null $H_0^{(0)}$ is insufficient. Moreover, as discussed in Section 6, rejection of $H_0^{(1)}$ in favor of $\theta < 1$ may motivate different standardization strategies when the primary goal is to understand changes in treatment efficacy.

In practice, $H_0 : \theta \in \{0, 1\}$ considers testing at both boundary points for θ , somewhat similar to testing variance components in mixed-effects models (Stram and Lee, 1994) and as such characterizing the asymptotic distribution of $\hat{\theta}$ under the null would likely yield a challenging ratio involving mixtures of chi-squared distributions. On the other hand, a full nonparametric bootstrap is computationally infeasible in our setting, given that the size of the pooled dataset \mathcal{D} exceeds several million eligible subject-trials for comparisons involving non-surgical patients (Figure S2). Not only does re-estimation of nuisance functions across bootstrapped datasets pose a large computational burden, but so too does prediction of $\hat{\mu}_m(a_m, \mathbf{L}_j)$ and $\hat{\xi}_{j,m}(\mathbf{L}_m)$ given that the number of predictions required is a M -fold larger than the size of \mathcal{D} .

Instead, we use an asymptotic version of the parametric bootstrap (Efron and Tibshirani, 1994, Van der Vaart, 2000) for \mathbf{S} . In particular, under the conditions of Theorem 4, $\sqrt{n}(\hat{\mathbf{S}} - \mathbf{S}) \xrightarrow{d} \mathcal{N}(0, \boldsymbol{\Sigma})$ where $\boldsymbol{\Sigma} \in \mathbb{R}^{M^2 \times M^2}$ is the covariance matrix of \mathbf{S} , with entries $\boldsymbol{\Sigma}(s_{m_1 j_1}, s_{m_2 j_2}) = \text{Cov}[\dot{\chi}_{j_1, m_1}^*(O; P), \dot{\chi}_{j_2, m_2}^*(O; P)]$. Critically, this asymptotic normality for \mathbf{S} holds even when θ is at a boundary point. Letting $\hat{\boldsymbol{\Sigma}}_n$ denote the empirical covariance matrix of cross-trial influence function contributions, we resample $\hat{\mathbf{S}}^{(1)}, \dots, \hat{\mathbf{S}}^{(B)} \sim \mathcal{N}(\hat{\mathbf{S}}, \hat{\boldsymbol{\Sigma}}_n)$. Finally, to approximate the sampling distribution of $\hat{\theta}$, summarize resamples $\hat{\mathbf{S}}^{(1)}, \dots, \hat{\mathbf{S}}^{(B)}$ by their corresponding variance ratios $\hat{\theta}^{(1)}, \dots, \hat{\theta}^{(B)}$.

Unfortunately, due to the boundary null, bootstrapped replicates $\hat{\theta}^{(1)}, \dots, \hat{\theta}^{(B)}$ will never be exactly 0 or 1 and thus 95% percentile-based confidence intervals would never reject H_0 . We follow

a similar strategy to that of [Cavaliere et al. \(2022\)](#), and modify our test to allow for a small margin away from the boundary. For some small $\delta > 0$, we adopt the test $H_0^{(\delta)} : \theta \in [0, \delta] \cup [1 - \delta, 1]$ versus $H_1^{(\delta)} : \theta \in (\delta, 1 - \delta)$, and reject $H_0^{(\delta)}$ if a 95% percentile-based confidence interval is fully within $(\delta, 1 - \delta)$. One can interpret δ as the fraction of variability in entries in \mathbf{S} for which relative changes in causal effects is deemed negligible. The choice of δ is highly context dependent, as what constitutes clinically meaningful changes is application specific; in the present context of bariatric surgery, we adopt $\delta = 0.05$.

6 Practical Guidance for How and Why Effects Vary

Thus far, we have introduced statistical tools to characterize *how* treatment effects change across the study entry period, along with summary measures to quantify the role of covariate shift in explaining *why* effects might change. In our experience, each set of tools in isolation reflects an incomplete picture, and both are necessary to inform analysts how best to understand and report findings. Although the goals of each study differ, and we do not advocate for a “one size fits all” approach, [Section 6.1](#) and [Table 1](#) summarize how analysts might use tools from this work to help interpret, characterize, and report calendar time-varying effects in their study.

Under [Assumptions 1-4](#) and the conditions of [Theorems 2](#) and [4](#), the only possible explanations for changes in treatment effects over calendar time are due to covariate shift in effect modifiers or changes in underlying treatment efficacy. [Section 6.2](#) comments on alternative explanations under violations of these assumptions.

6.1 Guidance Under No Violations of [Assumptions 1-4](#)

To illustrate how model selection and hypothesis testing for θ can be used together to understand reporting of calendar time-varying effects, we consider two scenarios, one where a constant MSM is selected and a second where a non-constant MSM is selected. First, when the selected MSM is a constant, it is reasonable to report a common effect for the study population, $\psi(m; \hat{\boldsymbol{\beta}}) = \hat{\beta}$, regardless of the value of θ . In some settings, $H_0^{(0)} : \theta = 0$ might be rejected despite a constant MSM having been selected. Such cases typically arise when differences in estimated treatment effects across calendar time are very small and manifest as random deviations centered around a common

effect. Altogether, selecting a constant MSM indicates minimal heterogeneity in the underlying effect over calendar time, suggesting that any observed variation is unlikely to be clinically meaningful.

If the selected MSM is non-constant across calendar time but $\theta \approx 0$, analysts should at minimum acknowledge that changes across time are driven by shifting underlying populations. This is particularly important when reporting a common effect, which implicitly reflects an averaged effect over these different populations across time. Alternatively, if $\theta \approx 1$, effect modification is not of concern, and it is appropriate to report $\psi(m; \hat{\beta})$ as the best estimate of the calendar time-varying treatment effect. While this is still reasonable if $\theta \in (0, 1)$, additional clarification should be reported to qualify that some amount of observed variation is due to effect modification. If there is particular interest in reporting on changes in treatment efficacy, one might consider standardization to a fixed population and report on the trend in that population (e.g., with an analogous projection-based curve). There are numerous reasonable choices for this fixed population, including both the most recent target trial population(s) (e.g., if they best represent subjects currently receiving treatment), or a subgroup defined by levels of key effect modifiers (e.g., patients with diabetes)

6.2 Guidance under Unmeasured Confounding or Model Misspecification

Including m as a covariate in nonparametric pooled models can make it difficult to disentangle differential forms of bias across trials from changes in the treatment effect over calendar time, i.e., it can be that $\hat{\theta}$ is greater than 0 even if the underlying treatment efficacy itself is not changing. Under violations of Assumptions 3, for example, the difference between $\hat{\chi}_{j,m_1}$ and $\hat{\chi}_{j,m_2}$ would reflect both the difference in treatment efficacy between times m_1 and m_2 but also the difference in bias introduced by unmeasured confounding. A similar phenomenon holds under nuisance model misspecification such that trial index covariate captures residual confounding. It is exactly for these reasons why reliance on θ on its own is inadequate to characterize changing treatment efficacy. Though biases may introduce small differences between $\hat{\chi}_{j,m_1}$ and $\hat{\chi}_{j,m_2}$ even when $\chi_{j,m_1}(P) = \chi_{j,m_2}(P)$ (i.e. producing $\hat{\theta} > 0$), a constant projection MSM will still be selected if differences between treatment effect estimates across calendar time are insubstantial. Ultimately if there is a strong concern of wrongful attribution of credit towards changes in underlying treatment efficacy, one can choose a larger value of c in the projection MSM selection procedure, thereby enforcing that changes in $\hat{\chi}_m$ over time must be greater in order for a non-constant MSM to be selected.

Projection Model: Constant ($\psi(m, \beta) = \beta$)			
	Fail to Reject $H_0^{(\delta)}$ ($\theta \leq \delta$)	Fail to Reject $H_0^{(\delta)}$ ($\theta \geq 1 - \delta$)	Reject $H_0^{(\delta)}$ ($\theta \in (\delta, 1 - \delta)$)
Calendar Time Varying Effect (Study Population)	X	X	X
Calendar Time Varying Effect (Fixed Population)	X	\checkmark^*	\checkmark^*
Reason(s) for Variation	No Variation	*Variation not clinically meaningful	*Variation not clinically meaningful
Action	Report common effect	Report common effect	Report common effect
Projection Model: Not Constant ($\psi(m, \beta) \neq \beta$)			
	Fail to Reject $H_0^{(\delta)}$ ($\theta \leq \delta$)	Fail to Reject $H_0^{(\delta)}$ ($\theta \geq 1 - \delta$)	Reject $H_0^{(\delta)}$ ($\theta \in (\delta, 1 - \delta)$)
Calendar Time Varying Effect (Study Population)	\checkmark	\checkmark	\checkmark
Calendar Time Varying Effect (Fixed Population)	X	\checkmark	\checkmark
Reason(s) for Variation	Covariate shift in effect modifiers	Possible changes in treatment efficacy	Covariate shift in effect modifiers, possible changes in treatment efficacy
Action	Acknowledge changes across time driven by changes in underlying populations Consider standardization to fixed population and reporting common effect in that population	Report calendar time-varying effect	Report calendar time-varying effect Consider standardization to fixed population to further study changes in treatment efficacy

Table 1: Summary of possible reporting decisions based on joint results from projection marginal structural model and θ .

6.3 Simulations

Extensive simulations, tied closely to the motivating study of bariatric surgery, which validate the utility of the tools outlined in Sections 4 and 5, are provided in Appendix S3. Simulations highlight how MSM model selection varies by sample size and choice of shrinkage parameter c , along with the ability of the inferential procedure described in 5.5 to distinguish between effect modification from underlying variation in treatment efficacy.

7 Application of Framework to Bariatric Surgery

Finally, we return to our motivating study of bariatric surgery and apply the proposed methods to examine trends over calendar time from 2005 to 2011. Analyses were conducted across 16 settings,

defined by four post-surgical follow-up times (6 months, 1 year, 2 years, and 3 years) and four treatment comparisons (no surgery versus surgery, no surgery versus RYGB or SG separately, and RYGB versus SG). No SG patients met study eligibility criteria until month $m = 30$, so analysis for comparisons involving SG was restricted to trials $m \in \{30, \dots, 84\}$.

Random forests were used to estimate all pooled nuisance models, separately for each setting, adjusting for age, BMI, sex, race, KP study site, self-reported smoking status, hypertension, dyslipidemia, type II diabetes, and prescriptions for antilipemic or antihypertensive medications, or insulin. This set of potential confounders directly followed from those used by [Arterburn et al. \(2020\)](#). Candidate MSMs for projection included constant, linear, and cubic models, and splines with 2 and 3 internal knots. To select among candidate MSMs, we employed the procedure described in Section 4.4 with $c = 0.25$. Additional details on precise covariate and outcome definitions, as well as results for other choices of c , are provided in the Supplementary Materials.

Figure 3A presents estimated differences in mean relative weight change across calendar time. Gray points denote trial-specific ATEs, $\hat{\chi}_m$, and overlaid lines denote estimated trends, $\psi(m; \hat{\beta})$, from each candidate MSM. As summarized in Table 2, non-constant MSMs were selected for all outcomes involving comparisons between surgery versus no surgery, and RYGB versus no surgery, as well as for the 6-month weight change outcome in comparisons involving SG.

Based on selected MSMs, surgical patients experienced excess 3-year weight change (relative to non-surgical patients) of -27.4% (-30.1%, -24.8%) at $m = 1$ and -18.3% (-18.8%, -17.8%) at $m = 84$, reflecting a change of 9.1% estimated treatment effect between 2005 and 2011. This temporal shift indicates that the common effect of -19.6% reported in Section 2, obtained by projection onto a constant MSM, obscures an important aspect understanding the efficacy of bariatric surgery.

Similar changes were observed for RYGB patients, with estimated 3-year weight change differences ranging from -28.3% (-31.3%, -25.3%) at $m = 1$ to -23.0% (-23.5%, -22.5%) at $m = 84$. As reflected in Figure 3, there is little change in the 3-year RYGB effect estimate after $m = 20$. Unsurprisingly then, the common effect estimate of -23.1% reported in Section 2 is comprises a reasonable summary of the treatment effect for a much greater portion of the study period.

A constant MSM was selected for the 3-year weight change outcome comparing SG patients relative to non-surgical patients. Thus, the reported estimate of -16.3% from Section 2 already reflects what one might reasonably report, after considering the possibility of variation over calendar

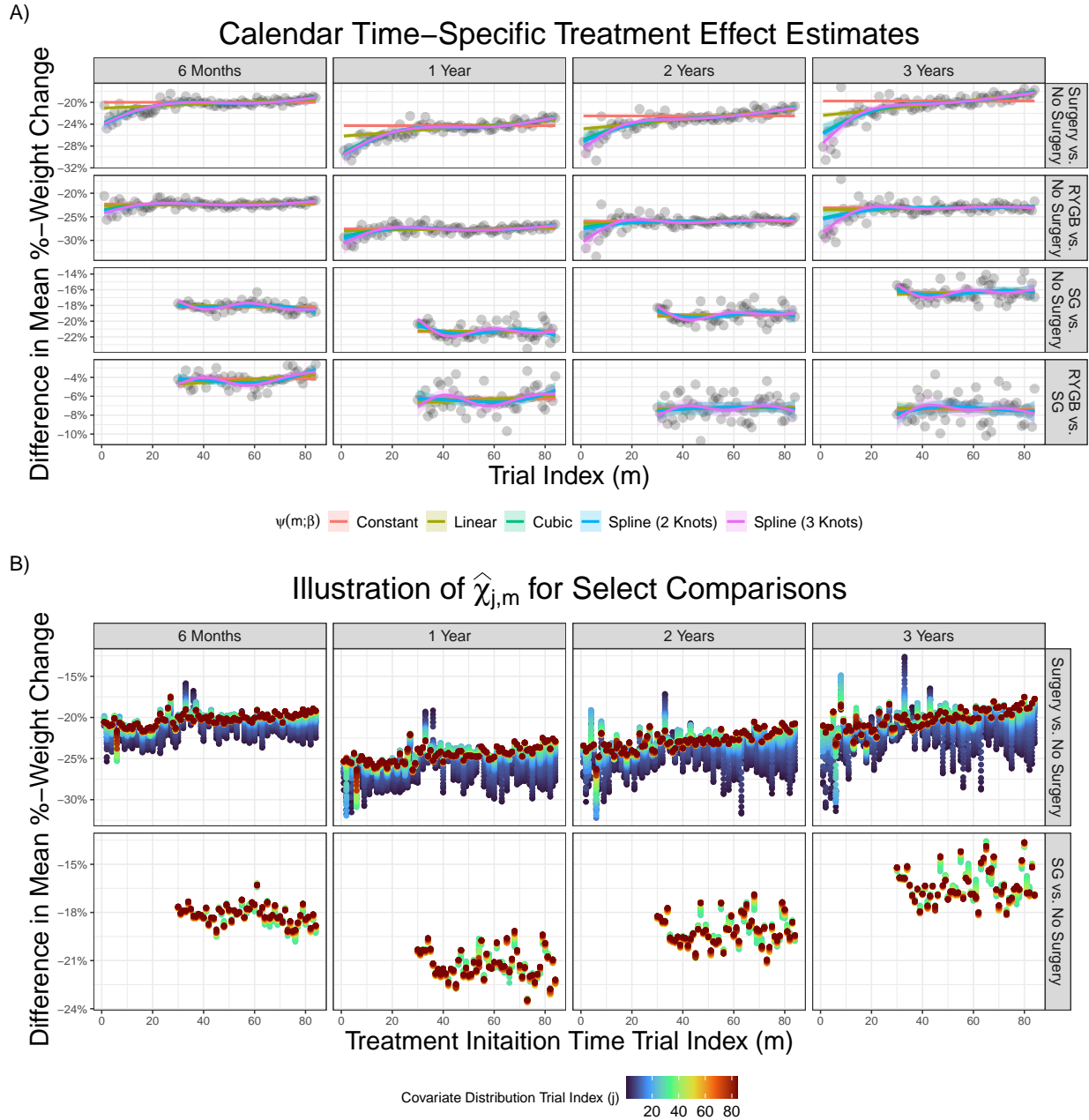


Figure 3: (A) Estimates of calendar time-specific treatment effects $\hat{\chi}_m$ (dots) and trends based on five candidate marginal structural models, $\psi(m; \hat{\beta})$. (B) Estimates of cross-trial effects $\hat{\chi}_{j,m}$ for select comparisons.

time. Non-constant MSMs were selected in other comparisons involving SG patients, however, as 6-month weight change treatment effects for SG patients between $m = 30$ and $m = 84$ improved by 1.0% [-17.5% (-17.7%, -17.2%) to -18.5% (-19.0%, -17.9%)] compared to non-surgical patients, and by 1.3% [4.7 (4.0, 5.5)% to 3.4% (2.8%, 4.0%)] compared to patients undergoing RYGB.

Figure 3B presents estimates of $\hat{\chi}_{j,m}$ for select comparisons. For a fixed m , variation in the verti-

Comparison	Outcome	Minimizing MSM	Selected MSM	95% Interval for θ
Surgery vs. No Surgery	6 Months	Spline (3 Knots)	Cubic	(0.684, 0.809)
	1 Year	Spline (3 Knots)	Spline (3 Knots)	(0.648, 0.767)
	2 Years	Spline (2 Knots)	Spline (2 Knots)	(0.644, 0.765)
	3 Years	Spline (3 Knots)	Spline (3 Knots)	(0.682, 0.777)
RYGB vs. No Surgery	6 Months	Cubic	Cubic	(0.668, 0.821)
	1 Year	Spline (3 Knots)	Spline (3 Knots)	(0.658, 0.795)
	2 Years	Spline (3 Knots)	Spline (3 Knots)	(0.647, 0.785)
	3 Years	Spline (3 Knots)	Spline (3 Knots)	(0.670, 0.787)
SG vs. No Surgery	6 Months	Spline (3 Knots)	Spline (3 Knots)	(0.971, 0.989)
	1 Year	Constant	Constant	(0.974, 0.991)
	2 Years	Linear	Constant	(0.980, 0.992)
	3 Years	Constant	Constant	(0.979, 0.992)
RYGB vs. SG	6 Months	Spline (3 Knots)	Cubic	(0.718, 0.807)
	1 Year	Constant	Constant	(0.670, 0.784)
	2 Years	Constant	Constant	(0.666, 0.784)
	3 Years	Constant	Constant	(0.688, 0.793)

Table 2: Summary of model selection results and 95% bootstrapped intervals for θ . The minimizing MSM denotes $\hat{\psi}^*$ minimizing $\hat{L}(\hat{\psi})$, while the selected MSM denotes the simplest model within $c = 0.25$ weighted standard deviations of the minimizer.

cal direction reflects changes in cross-trial effects when varying the underlying population (captured by $\hat{\gamma}_m^2$). Conversely, for a fixed color, variation in the height of points reflects changes in cross-trial effects in a particular population across calendar time (captured by $\hat{\sigma}_m^2$). Notably, the greater degree of variation in the vertical direction at fixed points in time (i.e., when varying populations) in the top row of Figure 3B suggests that covariate shift plays a larger role in explaining trends across calendar time for comparisons of no surgery to all surgical procedures than to SG alone. This is further reflected by 95% confidence intervals for θ in Table 2, which reject $H_0^{(\delta)}$ in all comparisons except those between SG and no surgery (with $\delta = 0.05$).

It is not overly surprising that underlying treatment efficacy for bariatric surgery relative to no surgery appears to have “declined” over time, given that the composition of bariatric procedures, specifically the proportion of RYGB and SG, has itself changed over time. Nevertheless, that our method is able to discover this well-explained trend offers evidence of its utility. When making comparisons to non-surgical patients, much of the clinical literature aggregates all surgical procedures under a single label “bariatric surgery” (Benz et al., 2024, Fisher et al., 2018, Haneuse et al., 2025, Harrington et al., 2024, Madenci et al., 2024, O’Brien et al., 2018). As such, recognizing that both the meaning and the underlying effectiveness of this aggregated treatment label have changed is particularly relevant. Our results also hint at possible improvements in SG technique and improved weight loss outcomes 6-months post surgery, though such improvements are not observed for longer-

term outcomes. One possible explanation is that any underlying changes in technique have helped patients reach their weight-loss nadir more quickly, but have not influenced peak weight-loss or rebound effects (Arterburn et al., 2020, Courcoulas et al., 2013).

8 Discussion

Observational studies leveraging EHR data are inherently subject to many factors beyond the control of investigators, particularly with respect to how treatments are administered and to whom. When a study reports a single causal effect (e.g., “the” ATE), that estimate implicitly reflects an average of calendar time-specific effects, which may not themselves be constant over time. Although the appropriate structure of reported effects depends largely on the goals of a given study, the methods in this work are designed to clarify both *how* and *why* causal effects may vary across calendar time. In doing so, the intent is that they will help guide decisions about what to report, particularly when potential changes to underlying treatment efficacy over time are of interest.

One key benefit of the sequential target trial approach considered in this work is that the design directly establishes initiator cohorts (i.e., each with a common time zero), through which calendar time-specific treatment effects can be defined. The proposed methods generalize to other study designs, however, provided that the study entry period can be discretized into sufficiently narrow windows through which one can define calendar time-specific effects. For example, head-to-head comparisons of RYGB and SG do not strictly require a sequence of target trials because the start of follow-up is defined by the date of surgery, and a (matched) cohort design may be a reasonable alternative (Benz et al., 2025, McTigue et al., 2020). Under such designs, one might partition the study entry period into small intervals and define contrasts analogous to $\chi_m(P)$ and $\chi_{j,m}(P)$, before applying the ideas introduced in this work. The choice of interval length will be application specific, and depend on both how quickly clinical practice can change as well as the frequency of treatment.

In studies where there is no clinical rationale for changes in underlying treatment efficacy (e.g., when treatments are fixed-dose pharmaceutical medications), summarizing variation in cross-trial effects can serve as a useful diagnostic for detecting effect modification over time. For instance, θ may be particularly informative in pharmacoepidemiologic studies, helping to quantify how treatment effects vary as the characteristics of medication users evolve with broader adoption.

We note that there are natural connections between our work and prior work on violations of the consistency assumption in causal inference (Cole and Frangakis, 2009, VanderWeele, 2009, VanderWeele and Hernán, 2013). While RYGB and SG can be framed as multiple versions of bariatric surgery, it is perhaps less natural to view each procedure over time as multiple versions of treatment in the usual sense, in part because it is rarely known when treatments differ, and thus which “version” of treatment was received. In a sense, our setup implicitly defines trial-specific versions of treatment, i.e., through the symbols A_m and a_m . However, we choose to view counterfactual outcomes $Y_m(a_m)$ similarly to those defined and framed in Cole and Frangakis (2009), $Y(a, k)$, where the additional treatment details (k) required to maintain consistency are entirely captured by trial index (m) in our notation. In particular, we adopt the viewpoint that if $a_m = a_j$ but $Y_m(a_m) \neq Y_j(a_j)$, then this reflects changes in the efficacy of a particular treatment a between two time points m, j , rather than always calling this phenomenon multiple versions of treatment. This choice is in line with Cole and Frangakis, who note that taking versions of treatment to the extreme precludes any sort of generalizability and hampers the utility of a study.

Finally, we have assumed throughout that during the time period where a patient is enrolled in Kaiser Permanente insurance, and thus is accessible in the EHR, there is no missing data in components of O . In practice, missing covariates may preclude ascertainment of eligibility, or outcomes may be missing even when eligibility is ascertainable. For the purposes of this work, we treat patients with incomplete information at a particular trial as ineligible ($E_m = 0$). However, we see combining ideas from our framework with recent work on causal inference under missing eligibility (Benz et al., 2024, 2025) as key area of future research. Simultaneously handling possibly missing treatment status and/or outcomes across trials represents another important line of further methodological development.

Code Availability

All code for analysis and simulations is made available on GitHub at https://github.com/lbenz730/calendar_time.

Acknowledgments

This work was supported by NIH Grants R01 DK128150-01, R01 HL166324, and F31 DK141237-01

References

- D. Arterburn and A. Courcoulas. Bariatric surgery for obesity and metabolic conditions in adults. *BMJ*, 349:g3961, 2014.
- David E Arterburn, Eric Johnson, Karen J Coleman, Lisa J Herrinton, Anita P Courcoulas, David Fisher, Robert A Li, Mary Kay Theis, Liyan Liu, James R Fraser, et al. Weight outcomes of sleeve gastrectomy and gastric bypass compared to nonsurgical treatment. *Annals of Surgery*, 274(6):e1269–e1276, 2020.
- Luke Benz, Rajarshi Mukherjee, Rui Wang, David Arterburn, Heidi Fischer, Catherine Lee, Susan M Shortreed, and Sebastien Haneuse. Adjusting for selection bias due to missing eligibility criteria in emulated target trials. *American Journal of Epidemiology*, page kwae471, 2024.
- Luke Benz, Rajarshi Mukherjee, Rui Wang, David Arterburn, Heidi Fischer, Catherine Lee, Susan M. Shortreed, Sebastien Haneuse, and Alexander W. Levis. Robust causal inference for ehr-based studies of point exposures with missingness in eligibility criteria, 2025. URL <https://arxiv.org/abs/2504.16230>.
- Lauren E. Cain, James M. Robins, Emilie Lanoy, Roger Logan, Dominique Costagliola, and Miguel A. Hernán. When to start treatment? a systematic approach to the comparison of dynamic regimes using observational data. *International Journal of Biostatistics*, 6(2):Article 18, 2010.
- Brantly Callaway and Pedro H.C. Sant’Anna. Difference-in-differences with multiple time periods. *Journal of Econometrics*, 225(2):200–230, 2021. ISSN 0304-4076. doi: 10.1016/j.jeconom.2021.03.012.
- Ellen C Caniglia, Rebecca Zash, Catherine Fennell, et al. Emulating target trials to avoid immortal time bias - an application to antibiotic initiation and preterm delivery. *Epidemiology*, 34(3):430–438, 2023.
- Joan A. Casey, Brian S. Schwartz, Walter F. Stewart, and Nancy E. Adler. Using electronic health records for population health research: A review of methods and applications. *Annual Review of Public Health*, 37:61–81, 2016. doi: 10.1146/annurev-publhealth-032315-021353. URL <https://doi.org/10.1146/annurev-publhealth-032315-021353>. Epub 2015 Dec 11.
- Giuseppe Cavaliere, Heino Bohn Nielsen, Rasmus Søndergaard Pedersen, and Anders Rahbek. Bootstrap inference on the boundary of the parameter space, with application to conditional volatility models. *Journal of Econometrics*, 227(1):241–263, 2022. doi: 10.1016/j.jeconom.2020.05.006. URL <https://doi.org/10.1016/j.jeconom.2020.05.006>.
- Victor Chernozhukov, Denis Chetverikov, Mert Demirer, et al. Double/debiased machine learning for treatment and structural parameters. *The Econometrics Journal*, 21(1):C1–C68, 01 2018.
- Stephen R. Cole and Constantine E. Frangakis. The consistency statement in causal inference: A definition or an assumption? *Epidemiology*, 20(1):3–5, 2009. doi: 10.1097/EDE.0b013e31818ef366.
- K. J. Coleman, Y. H. Shu, H. Fischer, et al. Bariatric surgery and risk of death in persons with chronic kidney disease. *Annals of Surgery*, 276(6):e784–e791, 2022. doi: 10.1097/SLA.0000000000004851.
- Karen J. Coleman, Sebastien Haneuse, Eric Johnson, et al. Long-term microvascular disease outcomes in patients with type 2 diabetes after bariatric surgery: Evidence for the legacy effect of surgery. *Diabetes care*, 39(8):1400–1407, 2016. doi: 10.2337/dc16-0194.

- Anita P Courcoulas, Nadine J Christian, Steven H Belle, et al. Weight change and health outcomes at 3 years after bariatric surgery among individuals with severe obesity. *JAMA*, 310(22):2416–2425, 2013.
- Anita P. Courcoulas, M. E. Patti, B. Hu, D. E. Arterburn, et al. Long-term outcomes of medical management vs bariatric surgery in type 2 diabetes. *JAMA*, 331(8):654–664, 2024.
- RB D’Agostino, ML Lee, AJ Belanger, LA Cupples, K Anderson, and WB Kannel. Relation of pooled logistic regression to time dependent cox regression analysis: the framingham heart study. *Statistics in Medicine*, 9(12):1501–1515, 1990.
- Issa J Dahabreh, Sarah E Robertson, Eric J Tchetgen, Elizabeth A Stuart, and Miguel A Hernán. Generalizing causal inferences from individuals in randomized trials to all trial-eligible individuals. *Biometrics*, 75(2):685–694, 2019.
- Issa J Dahabreh, Sarah E Robertson, Jon A Steingrimsson, Elizabeth A Stuart, and Miguel A Hernan. Extending inferences from a randomized trial to a new target population. *Statistics in Medicine*, 39(14):1999–2014, 2020.
- Goodarz Danaei, Luis A Rodríguez, Ofelia F Cantero, Roger Logan, and Miguel A Hernán. Observational data for comparative effectiveness research: an emulation of randomised trials of statins and primary prevention of coronary heart disease. *Statistical methods in medical research*, 22(1):70–96, 2013.
- Barbra A. Dickerman, Xabier García-Albéniz, Roger W. Logan, and et al. Avoidable flaws in observational analyses: An application to statins and cancer. *Nature Medicine*, 25(10):1601–1606, 2019. doi: 10.1038/s41591-019-0597-x.
- Piyemeth Dilokthornsakul, Nathorn Chaiyakunapruk, Glen T. Schumock, and Todd A. Lee. Calendar time-specific propensity score analysis for observational data: a case study estimating the effectiveness of inhaled long-acting beta-agonist on asthma exacerbations. *Pharmacoepidemiology and Drug Safety*, 23(2):152–164, 2014. ISSN 1053-8569. doi: 10.1002/pds.3540. URL <https://doi.org/10.1002/pds.3540>.
- Stacie B. Dusetzina, Christina D. Mack, and Til Stürmer. Propensity score estimation to address calendar time-specific channeling in comparative effectiveness research of second generation antipsychotics. *PLOS ONE*, 8(5):e63973, 2013. doi: 10.1371/journal.pone.0063973. URL <https://doi.org/10.1371/journal.pone.0063973>.
- Iván Díaz, Nicholas Williams, and Edward J. Hoffman Katherine L., Schenck. Nonparametric causal effects based on longitudinal modified treatment policies. *Journal of the American Statistical Association*, 118(542):846–857, 2023.
- Bradley Efron and Robert J. Tibshirani. *An Introduction to the Bootstrap*. Chapman & Hall/CRC, New York, NY, 1994. ISBN 0412042312, 9780412042317.
- G. R. Faria. A brief history of bariatric surgery. *Porto Biomedical Journal*, 2(3):90–92, May-Jun 2017. doi: 10.1016/j.pbj.2017.01.008.
- D. M. Felsenreich, E. Artemiou, K. Steinlechner, et al. Fifteen years after sleeve gastrectomy: Weight loss, remission of associated medical problems, quality of life, and conversions to roux-en-y gastric bypass—long-term follow-up in a multicenter study. *Obesity Surgery*, 31:3453–3461, 2021. doi: 10.1007/s11695-021-05475-x. URL <https://doi.org/10.1007/s11695-021-05475-x>.

- D. P. Fisher, E. Johnson, S. Haneuse, D. Arterburn, K. J. Coleman, P. J. O'Connor, R. O'Brien, A. Bogart, M. K. Theis, J. Anau, E. B. Schroeder, and S. Sidney. Association between bariatric surgery and macrovascular disease outcomes in patients with type 2 diabetes and severe obesity. *JAMA*, 320(15):1570–1582, 2018. doi: 10.1001/jama.2018.14619.
- Joshua J. Gagne, Katsiaryna Bykov, Richard J. Willke, Karl-Heinz Kahler, Pranav Subedi, and Sebastian Schneeweiss. Treatment dynamics of newly marketed drugs and implications for comparative effectiveness research. *Value in Health*, 16(6):1054–1062, 2013. ISSN 1098-3015. doi: 10.1016/j.jval.2013.06.012. URL <https://doi.org/10.1016/j.jval.2013.06.012>.
- Michel Gagner, Mervyn Deitel, Thomas L. Kalberer, et al. The second international consensus summit for sleeve gastrectomy, march 19–21, 2009. *Surgery for Obesity and Related Diseases*, 9(1):89–99, 2013. doi: 10.1016/j.soard.2012.10.007.
- Malini Gokhale, John B. Buse, DeFilippo Mack, et al. Calendar time as an instrumental variable in assessing the risk of heart failure with antihyperglycemic drugs. *Pharmacoepidemiology and Drug Safety*, 27(8):857–866, 2018. ISSN 1053-8569. doi: 10.1002/pds.4578. URL <https://doi.org/10.1002/pds.4578>.
- Cem Emir Guldogan, Omer Vefik Ozozan, and Mehmet Mahir Ozmen. Sleeve gastrectomy and its modifications. *Annals of Laparoscopic and Endoscopic Surgery*, 5(1):27, 2020. doi: 10.21037/ales-20-30. URL <https://ales.amegroups.org/article/view/5933>. Received: 02 February 2020; Accepted: 27 April 2020; Published: 20 July 2020.
- Sebatien Haneuse, Luke Benz, Valerie A. Smith, David Arterburn, and Matthew L. Maciejewski. Long-term cardiovascular outcomes following bariatric surgery: Reconciling seemingly conflicting evidence. *Epidemiology*, 2025. In press.
- L. B. Harrington, L. Benz, S. Haneuse, et al. Bariatric surgery and the long-term risk of venous thromboembolism: A population-based cohort study. *Obesity Surgery*, 34(6):2017–2025, 2024. doi: 10.1007/s11695-024-07236-y.
- Boudewijn Hasselman. *nleqslv: Solve Systems of Nonlinear Equations*, 2023. URL <https://cran.r-project.org/package=nleqslv>. R package version 3.3.5.
- Arja Helin-Salmivaara, Pirjo Lavikainen, Emma Aarnio, et al. Sequential cohort design applying propensity score matching to analyze the comparative effectiveness of atorvastatin and simvastatin in preventing cardiovascular events. *PLoS ONE*, 9(3):e90325, 2014.
- Miguel A Hernán, Brian C Sauer, Sonia Hernández-Díaz, Robert Platt, and Ian Shrier. Specifying a target trial prevents immortal time bias and other self-inflicted injuries in observational analyses. *Journal of Clinical Epidemiology*, 79:70–75, 2016.
- MA Hernán and J Robins. *Causal Inference: What if*. Boca Raton: Chapman & Hall/CRC, 2024.
- Miguel Hernán and James Robins. Using big data to emulate a target trial when a randomized trial is not available. *American Journal of Epidemiology*, 183(8):758–764, 2016.
- Kaiser Permanente. Weight-loss (bariatric) surgery. <https://healthy.kaiserpermanente.org/health-wellness/health-encyclopedia/he.weight-loss-bariatric-surgery.abq5755>, 2023.
- Edward H. Kennedy. Semiparametric doubly robust targeted double machine learning: a review, 2023.

- Edward H. Kennedy, Scott A. Lorch, and Dylan S. Small. Robust causal inference with continuous instruments using the local instrumental variable curve. *Journal of the Royal Statistical Society: Series B (Statistical Methodology)*, 81(1):121–143, 2019. doi: 10.1111/rssb.12300.
- Edward H Kennedy, Sivaraman Balakrishnan, and Larry A Wasserman. Semiparametric counterfactual density estimation. *Biometrika*, 110(4):875–896, 2023. doi: 10.1093/biomet/asad017.
- N. Laiteerapong and E. S. Huang. The pace of change in medical practice and health policy: collision or coexistence? *Journal of General Internal Medicine*, 30(6):848–852, Jun 2015. doi: 10.1007/s11606-015-3182-0.
- KyungMann Lee, Elizabeth L. Turner, and Arlene Kenny. Analysis of stepped-wedge cluster randomized trials when treatment effects vary by exposure time or calendar time. *Statistics in Medicine*, 44(20-22):e70256, 2025. ISSN 0277-6715. doi: 10.1002/sim.70256. URL <https://doi.org/10.1002/sim.70256>.
- Christina D. Mack, Robert J. Glynn, M. Alan Brookhart, et al. Calendar time-specific propensity scores and comparative effectiveness research for stage iii colon cancer chemotherapy. *Pharmacoepidemiology and Drug Safety*, 22(8):810–818, Aug 2013. doi: 10.1002/pds.3386. URL <https://doi.org/10.1002/pds.3386>.
- A. L. Madenci, K. E. Kurgansky, B. A. Dickerman, et al. Estimating the effect of bariatric surgery on cardiovascular events using observational data? *Epidemiology (Cambridge, Mass.)*, 35(5): 721–729, 2024. doi: 10.1097/EDE.0000000000001765.
- Kathleen M. McTigue, Rebecca Wellman, Eric Nauman, et al. Comparing the 5-year diabetes outcomes of sleeve gastrectomy and gastric bypass: The pcornt bariatric study. *JAMA Surgery*, 155(10):1–9, 2020. doi: 10.1001/jamasurg.2020.2743.
- Romain Neugebauer and Mark J. Van der Laan. Nonparametric causal effects based on marginal structural models. *Journal of Statistical Planning and Inference*, 137(2):419–434, 2007. doi: 10.1016/j.jspi.2005.12.008.
- Paul E O’Brien, Leah MacDonald, Margaret Anderson, Leah Brennan, and Wendy A Brown. Long-term outcomes after bariatric surgery: fifteen-year follow-up of adjustable gastric banding and a systematic review of the bariatric surgical literature. *Annals of Surgery*, 257(1):87–94, 2013.
- R. O’Brien, E. Johnson, S. Haneuse, K. J. Coleman, P. J. O’Connor, D. P. Fisher, S. Sidney, A. Bogart, M. K. Theis, J. Anau, E. B. Schroeder, and D. Arterburn. Microvascular outcomes in patients with diabetes after bariatric surgery versus usual care: A matched cohort study. *Annals of Internal Medicine*, 169(5):300–310, 2018. doi: 10.7326/M17-2383.
- B. N. Reames, J. F. Finks, D. Bacal, A. M. Carlin, and J. B. Dimick. Changes in bariatric surgery procedure use in michigan, 2006-2013. *JAMA*, 312(9):959–961, 2014. doi: 10.1001/jama.2014.7651.
- Michael Rosenblum and Mark J Van der Laan. Targeted maximum likelihood estimation of the parameter of a marginal structural model. *The International Journal of Biostatistics*, 6:1–27, 2010.
- Raul J. Rosenthal, Amalia A. Diaz, Daniel Arvidsson, et al. International sleeve gastrectomy expert panel consensus statement: Best practice guidelines based on experience of > 12,000 cases. *Surgery for Obesity and Related Diseases*, 8(1):8–19, 2012. doi: 10.1016/j.soard.2011.10.019.

- Gianluca Scola, Anca Chis Ster, Daniel Bean, et al. Implementation of the trial emulation approach in medical research: a scoping review. *BMC Medical Research Methodology*, 23(1):186, 2023. doi: 10.1186/s12874-023-02000-9. URL <https://doi.org/10.1186/s12874-023-02000-9>.
- K. H. Sheetz, J. Claffin, and J. B. Dimick. Trends in the adoption of robotic surgery for common surgical procedures. *JAMA Network Open*, 3(1):e1918911, 2020. doi: 10.1001/jamanetworkopen.2019.18911.
- Daniel O. Stram and Jae W. Lee. Variance components testing in the longitudinal mixed effects model. *Biometrics*, 50(4):1171–1177, 1994.
- Masashi Sugiyama, Taiji Suzuki, and Takafumi Kanamori. *Density ratio estimation in machine learning*. Cambridge University Press, 2012.
- Samy Suissa, Erica E. M. Moodie, and Sophie Dell’Aniello. Prevalent new-user cohort designs for comparative drug effect studies by time-conditional propensity scores. *Pharmacoepidemiology and Drug Safety*, 26(4):459–468, 2017. ISSN 1053-8569. doi: 10.1002/pds.4169. URL <https://doi.org/10.1002/pds.4169>.
- Liyang Sun and Sarah Abraham. Estimating dynamic treatment effects in event studies with heterogeneous treatment effects. *Journal of Econometrics*, 225(2):175–199, 2021. ISSN 0304-4076. doi: 10.1016/j.jeconom.2020.09.006.
- Anastasios Tsiatis. *Semiparametric Theory and Missing Data*. Springer Series in Statistics. Springer, New York, 2006. ISBN 978-0-387-23498-0.
- Yasushi Tsujimoto, Tomoko Fujii, Yusuke Tsutsumi, et al. Minimal important changes in standard deviation units are highly variable and no universally applicable value can be determined. *Journal of Clinical Epidemiology*, 145:92–100, 2022. ISSN 0895-4356. doi: 10.1016/j.jclinepi.2022.01.017. URL <https://www.sciencedirect.com/science/article/pii/S0895435622000233>.
- Lawson Ung, Guanbo Wang, Sebastien Haneuse, Miguel A. Hernán, and Issa J. Dahabreh. Combining an experimental study with external data: study designs and identification strategies, 2025. URL <https://arxiv.org/abs/2406.03302>.
- Mark J. van der Laan and Sandrine Dudoit. Unified cross-validation methodology for selection among estimators and a general cross-validated adaptive epsilon-net estimator. Working Paper 130, U.C. Berkeley Division of Biostatistics Working Paper Series, University of California, Berkeley, April 2003. Earlier version: April 7, 2003.
- Aad W Van der Vaart. *Asymptotic statistics*, volume 3. Cambridge university press, 2000.
- Tyler J. VanderWeele. Concerning the consistency assumption in causal inference. *Epidemiology*, 20(6):880–883, 2009. doi: 10.1097/EDE.0b013e3181bd5638.
- Tyler J. VanderWeele and Miguel A. Hernán. Causal inference under multiple versions of treatment. *Journal of Causal Inference*, 1(1):1–20, 2013. doi: 10.1515/jci-2012-0002.
- Bingkai Wang, Xueqi Wang, and Fan Li. How to achieve model-robust inference in stepped wedge trials with model-based methods? *Biometrics*, 80(4), December 2024. doi: 10.1093/biomtc/ujae123.
- Larry Wasserman. *All of Nonparametric Statistics*. Springer Texts in Statistics. Springer, New York, 2006. doi: 10.1007/0-387-30623-4.

Supplementary Material for “A Statistical Framework for Understanding Causal Effects that Vary by Treatment Initiation Time in EHR-based Studies”

Luke Benz¹, Rajarshi Mukherjee¹, Rui Wang^{1,2,3}, David Arterburn⁴, Heidi Fischer⁵, Catherine Lee⁶, Susan M. Shortreed^{7,8}, Alexander W. Levis^{*9}, and Sebastien Haneuse^{*1}

¹Department of Biostatistics, Harvard T.H. Chan School of Public Health, Boston, MA, USA

²Department of Population Medicine, Harvard Pilgrim Health Care Institute, Boston, MA, USA

³Department of Population Medicine, Harvard Medical School, Boston, MA, USA

⁴Kaiser Permanente Washington Health Research Institute, Seattle, WA, USA

⁵Department of Research & Evaluation, Kaiser Permanente Southern California, Pasadena, CA, USA

⁶Department of Epidemiology and Biostatistics, University of California San Francisco, San Francisco, CA, USA

⁷Biostatistics Division, Kaiser Permanente Washington Health Research Institute, Seattle, WA, USA

⁸Department of Biostatistics, University of Washington School of Public Health, Seattle, WA, USA

⁹Department of Biostatistics, Epidemiology and Informatics, University of Pennsylvania, Philadelphia, PA, USA

December 23, 2025

Contents

S1 Proofs	2
S1.1 Influence Function of $\chi_m(P)$	2
S1.2 Influence Function of $\beta(P)$ (Proof of Theorem 1)	3
S1.3 Asymptotic Behavior of $\hat{\chi}_m$ and $\hat{\beta}$ (Proof of Theorem 2)	4
S1.4 Identification of $\chi_{j,m}(P)$ (Proof of Lemma 1)	5
S1.5 Influence Function of $\chi_{j,m}(P)$ (Proof of Theorem 3)	5
S1.6 Asymptotic Behavior of $\hat{\chi}_{j,m}$ (Proof of Theorem 4)	7
S2 Additional Data Application Details	7
S2.1 Variable Definitions	7
S2.2 Analytic Methods	9
S2.3 Additional Application Figures and Tables	10
S3 Simulations	12
S3.1 Simulation Overview	12
S3.2 Simulation Data Generating Process	13
S3.3 Analysis Methods	14
S3.4 Simulation Results	15
S3.5 Simulation Parameters	18

* denotes co-last author (AWL and SH)

Corresponding Author: Luke Benz (lukebenz@g.harvard.edu)

S1 Proofs

S1.1 Influence Function of $\chi_m(P)$

Lemma S1. For $m \in \{1, \dots, M\}$, $\chi_m(P)$ satisfies the von Mises expansion

$$\chi_m(\bar{P}) - \chi_m(P) = - \int \dot{\chi}_m^*(o; \bar{P}) dP(o) + R_m(\bar{P}, P)$$

with remainder term, with inputs omitted for brevity, is given by

$$R_m(\bar{P}, P) = \mathbb{E}_P \left[\frac{E_m}{\bar{P}(E_m = 1)} \left\{ \left(1 - \frac{\pi_m}{\bar{\pi}_m} \right) (\bar{\mu}_m^{(1)} - \mu_m^{(1)}) - \left(1 - \frac{1 - \pi_m}{1 - \bar{\pi}_m} \right) (\bar{\mu}_m^{(0)} - \mu_m^{(0)}) \right\} \right] + \left(\chi_m(\bar{P}) - \chi_m(P) \right) \left(1 - \frac{P(E_m = 1)}{\bar{P}(E_m = 1)} \right)$$

Proof.

$$\begin{aligned} R_m(\bar{P}, P) &= \chi_m(\bar{P}) - \chi_m(P) + \int \dot{\chi}_m^*(o; \bar{P}) dP(o) \\ &= \chi_m(\bar{P}) - \chi_m(P) + \mathbb{E}_P \left[\frac{\mathbf{1}(E_m = 1)}{\bar{P}(E_m = 1)} \left\{ \bar{\mu}_m(1, \mathbf{L}_m) - \bar{\mu}(0, \mathbf{L}_m) - \chi_m(\bar{P}) + \left(\frac{A_m}{\bar{\pi}_m(\mathbf{L}_m)} - \frac{1 - A_m}{1 - \bar{\pi}_m(\mathbf{L}_m)} \right) (Y_m - \bar{\mu}(A_m, \mathbf{L}_m)) \right\} \right] \\ &= \mathbb{E}_P \left[\frac{\mathbf{1}(E_m = 1)}{\bar{P}(E_m = 1)} \left\{ \bar{\mu}_m(1, \mathbf{L}_m) - \bar{\mu}(0, \mathbf{L}_m) - \chi_m(P) + \left(\frac{A_m}{\bar{\pi}_m(\mathbf{L}_m)} - \frac{1 - A_m}{1 - \bar{\pi}_m(\mathbf{L}_m)} \right) (Y_m - \bar{\mu}(A_m, \mathbf{L}_m)) \right\} \right] \\ &\quad + \left(\chi_m(\bar{P}) - \chi_m(P) \right) \left(1 - \frac{P(E_m = 1)}{\bar{P}(E_m = 1)} \right) \\ &= \mathbb{E}_P \left[\frac{\mathbf{1}(E_m = 1)}{\bar{P}(E_m = 1)} \left\{ \bar{\mu}_m(1, \mathbf{L}_m) - \bar{\mu}(0, \mathbf{L}_m) - (\mu_m(1, \mathbf{L}_m) - \mu(0, \mathbf{L}_m)) + \left(\frac{\pi_m(\mathbf{L}_m)}{\bar{\pi}_m(\mathbf{L}_m)} - \frac{1 - \pi_m(\mathbf{L}_m)}{1 - \bar{\pi}_m(\mathbf{L}_m)} \right) (\mu_m(A_m, \mathbf{L}_m) - \bar{\mu}(A_m, \mathbf{L}_m)) \right\} \right] \\ &\quad + \left(\chi_m(\bar{P}) - \chi_m(P) \right) \left(1 - \frac{P(E_m = 1)}{\bar{P}(E_m = 1)} \right) \end{aligned}$$

The last line follows from applying the g -formula identification result for $\chi_m(P)$, and applying iterated expectation twice, first on \mathbf{L}_m, A_m , and then just on \mathbf{L}_m . Combining terms and omitting inputs for brevity, we are left with the desired result.

$$R_m(\bar{P}, P) = \mathbb{E}_P \left[\frac{E_m}{\bar{P}(E_m = 1)} \left\{ \left(1 - \frac{\pi_m}{\bar{\pi}_m} \right) (\bar{\mu}_m^{(1)} - \mu_m^{(1)}) - \left(1 - \frac{1 - \pi_m}{1 - \bar{\pi}_m} \right) (\bar{\mu}_m^{(0)} - \mu_m^{(0)}) \right\} \right] + \left(\chi_m(\bar{P}) - \chi_m(P) \right) \left(1 - \frac{P(E_m = 1)}{\bar{P}(E_m = 1)} \right)$$

By the von Mises expansion in Lemma S1 and an application of Lemma 2 of [Kennedy et al. \(2023\)](#), it follows that $\dot{\chi}_m^*(O; P)$ is the nonparametric influence function of $\chi_m(P)$ at P . \square

S1.2 Influence Function of $\beta(P)$ (Proof of Theorem 1)

The characterizing equation

$$0 = \sum_{m=1}^M w(m)P(E_m = 1) \nabla_{\beta} \psi(m; \beta)|_{\beta=\beta(P)} [\chi_m(P) - \psi(m; \beta(P))]$$

is obtained by differentiating the loss function which defines $\beta(P)$ —this is permitted as we have assumed that $\psi(m; \beta)$ is differentiable in β . We will use this equation to deduce the influence function of $\beta(P)$. Recall from [Bickel et al. \(1993\)](#) and [van der Vaart \(2002\)](#) that the nonparametric influence function $\dot{\beta}^*(O; P)$ is the unique mean-zero finite variance function satisfying pathwise differentiability:

$$\left. \frac{d}{d\epsilon} \beta(P_{\epsilon}) \right|_{\epsilon=0} = \mathbb{E}_P \left(\dot{\beta}^*(O; P) u(O) \right),$$

for any regular parametric submodel $\{P_{\epsilon} : \epsilon \in [0, 1]\}$ such that $P_0 \equiv P$ with score function $u(O) = \left. \frac{d}{d\epsilon} \log dP_{\epsilon} \right|_{\epsilon=0}$. Choosing such a regular parametric submodel and differentiating the estimating equation, we have

$$\begin{aligned} 0 &= \left. \frac{d}{d\epsilon} \sum_{m=1}^M w(m)P_{\epsilon}(E_m = 1) \nabla_{\beta} \psi(m; \beta)|_{\beta=\beta(P)} [\chi_m(P) - \psi(m; \beta(P))] \right|_{\epsilon=0} \\ &+ \left. \frac{d}{d\epsilon} \sum_{m=1}^M w(m)P(E_m = 1) \nabla_{\beta} \psi(m; \beta)|_{\beta=\beta(P_{\epsilon})} [\chi_m(P) - \psi(m; \beta(P_{\epsilon}))] \right|_{\epsilon=0} \\ &+ \left. \frac{d}{d\epsilon} \sum_{m=1}^M w(m)P(E_m = 1) \nabla_{\beta} \psi(m; \beta)|_{\beta=\beta(P)} [\chi_m(P_{\epsilon}) - \psi(m; \beta(P))] \right|_{\epsilon=0}, \end{aligned}$$

by properties of the total derivative. The first summand is simply

$$\sum_{m=1}^M w(m) \mathbb{E}_P(E_m u(O)) \nabla_{\beta} \psi(m; \beta)|_{\beta=\beta(P)} [\chi_m(P) - \psi(m; \beta(P))],$$

where we interchanged the derivative and integral, and used the fact that $\frac{d}{dx} \log f(x) = \frac{\frac{d}{dx} f(x)}{f(x)}$ for any differentiable function f . The second summand is $\mathbf{V} \left. \frac{d}{d\epsilon} \beta(P_{\epsilon}) \right|_{\epsilon=0}$ by the chain rule, where

$$\begin{aligned} \mathbf{V} &= \sum_{m=1}^M w(m)P(E_m = 1) \left\{ \nabla_{\beta}^2 \psi(m; \beta)|_{\beta=\beta(P)} [\chi_m(P) - \psi(m; \beta(P))] \right. \\ &\quad \left. - \nabla_{\beta} \psi(m; \beta)|_{\beta=\beta(P)} [\nabla_{\beta} \psi(m; \beta)|_{\beta=\beta(P)}]^T \right\} \end{aligned}$$

as defined in the main text. The third summand is

$$\sum_{m=1}^M w(m)P(E_m = 1) \nabla_{\beta} \psi(m; \beta)|_{\beta=\beta(P)} \mathbb{E}_P(\dot{\chi}_m^*(O; P) u(O))$$

by the defining property of $\dot{\chi}_m^*(O; P)$. Combining terms and solving for $\left. \frac{d}{d\epsilon} \beta(P_{\epsilon}) \right|_{\epsilon=0}$, we find

$$\begin{aligned} \left. \frac{d}{d\epsilon} \beta(P_{\epsilon}) \right|_{\epsilon=0} &= -\mathbf{V}^{-1} \mathbb{E}_P \left(\sum_{m=1}^M w(m) \nabla_{\beta} \psi(m; \beta)|_{\beta=\beta(P)} \{ E_m [\chi_m(P) - \psi(m; \beta(P))] \right. \\ &\quad \left. + P[E_m = 1] \dot{\chi}_m^*(O; P) \} u(O) \right). \end{aligned}$$

Thus, after canceling terms, we have shown that

$$\begin{aligned} \hat{\beta}^*(O; P) = & -\mathbf{V}^{-1} \sum_{m=1}^M w(m) \nabla_{\beta} \psi(m; \beta)|_{\beta=\beta(P)} E_m \left\{ \mu_m(1, \mathbf{L}_m) - \mu_m(0, \mathbf{L}_m) \right. \\ & \left. + \left(\frac{A_m}{\pi_m(\mathbf{L}_m)} - \frac{1 - A_m}{1 - \pi_m(\mathbf{L}_m)} \right) (Y_m - \mu_m(A_m, \mathbf{L}_m)) - \psi(m; \beta(P)) \right\}. \end{aligned}$$

S1.3 Asymptotic Behavior of $\hat{\chi}_m$ and $\hat{\beta}$ (Proof of Theorem 2)

The asymptotic behavior of $\hat{\chi}_m$ is a special case of Theorem 4, proved in Appendix Section S1.6; note that $\xi_{m,m} \equiv 1$ and does not need to be estimated. We thus focus on $\hat{\beta}$. By definition, $\beta(P)$ solves $\mathbb{E}_P[\varphi(O; \beta, \eta(P))] = 0$ for β , where for any candidate nuisance functions $\bar{\eta} = \{(\bar{\mu}_m, \bar{\pi}_m)\}_{m=1}^M$,

$$\begin{aligned} \varphi(O; \beta, \bar{\eta}) = & \sum_{m=1}^M E_m w(m) \nabla_{\beta} \psi(m; \beta) \left\{ \bar{\mu}_m(1, \mathbf{L}_m) - \bar{\mu}_m(0, \mathbf{L}_m) \right. \\ & \left. + \left(\frac{A_m}{\bar{\pi}_m(\mathbf{L}_m)} - \frac{1 - A_m}{1 - \bar{\pi}_m(\mathbf{L}_m)} \right) (Y_m - \bar{\mu}_m(A_m, \mathbf{L}_m)) - \psi(m; \beta) \right\}. \end{aligned}$$

Similarly, $\hat{\beta}$ is the solution to the empirical estimating equation $\mathbb{P}_n[\varphi(O; \beta, \hat{\eta})] = 0$ in β . We make the following assumptions:

Assumption S1. For each $m \in \{1, \dots, M\}$, the following hold:

- (i) $\|\hat{\pi}_m - \pi_m\|_{(m)} + \sum_{a=0}^1 \|\hat{\mu}_m(a, \cdot) - \mu_m(a, \cdot)\|_{(m)} = o_P(1)$,
- (ii) $\epsilon \leq \hat{\pi}_m(\mathbf{L}_m)$, $\pi(\mathbf{L}_m) \leq 1 - \epsilon$ and $|Y_m|, |\hat{\mu}_m(a, \mathbf{L}_m)| \leq \epsilon^{-1}$ almost surely when $E_m = 1$,

and, moreover, $\hat{\beta} \xrightarrow{P} \beta(P)$.

Assumption S2. The function class $\{\varphi(o; \beta, \bar{\eta}) : \beta \in \mathbb{R}^k\}$ is Donsker in β , for each fixed $\bar{\eta}$.

Assumption S3. The map $\beta \mapsto \mathbb{E}_P(\varphi(O; \beta, \bar{\eta}))$ is differentiable at $\beta(P)$ uniformly in $\bar{\eta}$, the derivative matrix $\nabla_{\beta} \mathbb{E}_P(\varphi(O; \beta, \bar{\eta}))|_{\beta=\beta(P)} =: \mathbf{V}(\beta(P), \bar{\eta})$ is invertible, and $\mathbf{V}(\beta(P), \hat{\eta}) \xrightarrow{P} \mathbf{V}(\beta(P), \eta(P))$.

Note that

$$\mathbb{E}_P(\varphi(O; \beta, \bar{\eta})) = \sum_{m=1}^M w(m) P[E_m = 1] \nabla_{\beta} \psi(m; \beta) \left\{ \mathbb{E}_P \left[\frac{E_m}{P[E_m = 1]} B_m(\bar{\eta}, \eta(P)) \right] + \chi_m(P) - \psi(m; \beta) \right\},$$

where

$$B_m(\bar{\eta}, \eta(P)) = \{\bar{\mu}_m(1, \mathbf{L}_m) - \mu_m(1, \mathbf{L}_m)\} \left(1 - \frac{\pi_m(\mathbf{L}_m)}{\bar{\pi}_m(\mathbf{L}_m)} \right) - \{\bar{\mu}_m(0, \mathbf{L}_m) - \mu_m(0, \mathbf{L}_m)\} \left(1 - \frac{1 - \pi_m(\mathbf{L}_m)}{1 - \bar{\pi}_m(\mathbf{L}_m)} \right).$$

Thus, the map $\beta \mapsto \mathbb{E}_P(\varphi(O; \beta, \bar{\eta}))$ will be differentiable in β as we have assumed $\psi(m; \beta)$ is twice differentiable in β . Moreover, each candidate marginal structural model considered in the main text belongs to a finite-dimensional linear space of bounded functions, and thus satisfies the Donsker conditions in Assumption S2 (van der Vaart and Wellner, 1996).

With these assumptions in hand, we can directly apply Lemma 3 in Kennedy et al. (2023), a very general result regarding sample-split M -estimators that involve nuisance functions. In particular, under our assumptions,

$$\hat{\beta} - \beta(P) = -\mathbf{V}(\beta(P), \eta(P))^{-1} \mathbb{P}_n[\varphi(O; \beta(P), \eta(P))] + O_P(R_{n,\beta}) + o_P(n^{-1/2}),$$

where $R_{n,\beta} = \mathbb{E}_P\{\varphi(O; \beta(P), \hat{\eta}) - \varphi(O; \beta(P), \eta(P))\}$. Note that $\varphi(O; \beta(P), \eta(P)) = \hat{\beta}^\dagger(O; P)$ and $-\mathbf{V}^{-1}\hat{\beta}^\dagger(O; P) = \hat{\beta}^*(O; P)$. Further, observe that

$$R_{n,\beta} = \sum_{m=1}^m w(m) \nabla_{\beta} \psi(m; \beta)|_{\beta=\beta(P)} \mathbb{E}_P(E_m B_m(\hat{\eta}, \eta(P))).$$

It thus follows that $R_{n,\beta} \lesssim \sum_{m=1}^M \hat{R}_m$, concluding the proof.

S1.4 Identification of $\chi_{j,m}(P)$ (Proof of Lemma 1)

$$\begin{aligned} \chi_{j,m}(P) &= \int_{\mathcal{L}} \mathbb{E}[Y_m(a_m = 1) - Y_m(a_m = 0) \mid \mathbf{L}_m = \boldsymbol{\ell}, g(\mathbf{L}_m) = 1] dP_{\mathbf{L}_j|E_j=1}(\boldsymbol{\ell} \mid E_j = 1) \\ &= \int_{\mathcal{L}} \mathbb{E}[Y_m(a_m = 1) - Y_m(a_m = 0) \mid A_m, \mathbf{L}_m = \boldsymbol{\ell}, g(\mathbf{L}_m) = 1] dP_{\mathbf{L}_j|E_j=1}(\boldsymbol{\ell} \mid E_j = 1) \quad (\text{A2, A3}) \\ &= \int_{\mathcal{L}} \left(\mathbb{E}[Y_m \mid A_m = 1, \mathbf{L}_m = \boldsymbol{\ell}, g(\mathbf{L}_m) = 1] - \mathbb{E}[Y_m \mid A_m = 0, \mathbf{L}_m = \boldsymbol{\ell}, g(\mathbf{L}_m) = 1] \right) dP_{\mathbf{L}_j|E_j=1}(\boldsymbol{\ell} \mid E_j = 1) \quad (\text{A1}) \\ &= \int_{\mathcal{L}} \left(\mathbb{E}[Y_m \mid A_m = 1, \mathbf{L}_m = \boldsymbol{\ell}, E_m = 1] - \mathbb{E}[Y_m \mid A_m = 0, \mathbf{L}_m = \boldsymbol{\ell}, E_m = 1] \right) dP_{\mathbf{L}_j|E_j=1}(\boldsymbol{\ell} \mid E_j = 1) \quad (\text{A4}) \\ &= \int_{\mathcal{L}} \left(\mu_m(1, \boldsymbol{\ell}) - \mu_m(0, \boldsymbol{\ell}) \right) dP_{\mathbf{L}_j|E_j=1}(\boldsymbol{\ell} \mid E_j = 1) \\ &= \mathbb{E}[\mu_m(1, \mathbf{L}_j) - \mu_m(0, \mathbf{L}_j) \mid E_j = 1] \end{aligned}$$

S1.5 Influence Function of $\chi_{j,m}(P)$ (Proof of Theorem 3)

To prove Theorem 3, we begin by introducing the following lemma, which provides the von Mises expansion for $\chi_{j,m}(P)$.

Lemma S2. *The functional $\chi_{j,m}^{(a)}(P) := \mathbb{E}(\mu_m(a, \mathbf{L}_j) \mid E_j = 1)$ satisfies the following von Mises expansion:*

$$\chi_{j,m}^{(a)}(\bar{P}) - \chi_{j,m}^{(a)}(P) = - \int \dot{\chi}_{j,m}^{(a)}(o; \bar{P}) dP(o) + R_{j,m}^{(a)}(\bar{P}, P),$$

where

$$\begin{aligned} \dot{\chi}_{j,m}^{(a)}(O; P) &= \frac{E_j}{P[E_j = 1]} \{ \mu_m(a, \mathbf{L}_j) - \chi_{j,m}^{(a)}(P) \} \\ &\quad + \frac{E_m}{P[E_m = 1]} \frac{\mathbb{1}(A_m = a)}{\pi_m(\mathbf{L}_m)^a \{1 - \pi_m(\mathbf{L}_m)\}^{1-a}} \xi_{j,m}(\mathbf{L}_m) \{ Y_m - \mu_m(a, \mathbf{L}_m) \}, \end{aligned}$$

and

$$\begin{aligned} R_{j,m}^{(a)}(\bar{P}, P) &= \left\{ \chi_{j,m}^{(a)}(\bar{P}) - \chi_{j,m}^{(a)}(P) \right\} \left\{ 1 - \frac{P[E_j = 1]}{\bar{P}[E_j = 1]} \right\} \\ &\quad + \left\{ \frac{P[E_j = 1]}{\bar{P}[E_j = 1]} - \frac{P[E_m = 1]}{\bar{P}[E_m = 1]} \right\} \mathbb{E}_P \left(\frac{E_j}{P[E_j = 1]} \{ \bar{\mu}_m(a, \mathbf{L}_j) - \mu_m(a, \mathbf{L}_j) \} \right) \\ &\quad + \mathbb{E}_P \left(\frac{E_m}{\bar{P}[E_m = 1]} \left\{ a \frac{\pi_m(\mathbf{L}_m)}{\bar{\pi}_m(\mathbf{L}_m)} + (1-a) \frac{1 - \pi_m(\mathbf{L}_m)}{1 - \bar{\pi}_m(\mathbf{L}_m)} \right\} \{ \bar{\xi}_{j,m}(\mathbf{L}_m) - \xi_{j,m}(\mathbf{L}_m) \} \{ \mu_m(a, \mathbf{L}_m) - \bar{\mu}_m(a, \mathbf{L}_m) \} \right) \\ &\quad + \mathbb{E}_P \left(\frac{E_m}{\bar{P}[E_m = 1]} \left\{ a \left(\frac{\pi_m(\mathbf{L}_m)}{\bar{\pi}_m(\mathbf{L}_m)} - 1 \right) + (1-a) \left(\frac{1 - \pi_m(\mathbf{L}_m)}{1 - \bar{\pi}_m(\mathbf{L}_m)} - 1 \right) \right\} \xi_{j,m}(\mathbf{L}_m) \{ \mu_m(a, \mathbf{L}_m) - \bar{\mu}_m(a, \mathbf{L}_m) \} \right). \end{aligned}$$

Proof. Observe that

$$\begin{aligned}
& \chi_{j,m}^{(a)}(\bar{P}) - \chi_{j,m}^{(a)}(P) + \mathbb{E}_P \left(\dot{\chi}_{j,m}^{(a)}(O; \bar{P}) \right) \\
&= \left\{ \chi_{j,m}^{(a)}(\bar{P}) - \chi_{j,m}^{(a)}(P) \right\} \left\{ 1 - \frac{P[E_j = 1]}{\bar{P}[E_j = 1]} \right\} \\
&\quad + \mathbb{E}_P \left(\frac{E_j}{\bar{P}[E_j = 1]} \{ \bar{\mu}_m(a, \mathbf{L}_j) - \mu_m(a, \mathbf{L}_j) \} \right. \\
&\quad \left. + \frac{E_m}{\bar{P}[E_m = 1]} \left\{ a \frac{\pi_m(\mathbf{L}_m)}{\bar{\pi}_m(\mathbf{L}_m)} + (1-a) \frac{1 - \pi_m(\mathbf{L}_m)}{1 - \bar{\pi}_m(\mathbf{L}_m)} \right\} \bar{\xi}_{j,m}(\mathbf{L}_m) \{ \mu_m(a, \mathbf{L}_m) - \bar{\mu}_m(a, \mathbf{L}_m) \} \right) \\
&= \left\{ \chi_{j,m}^{(a)}(\bar{P}) - \chi_{j,m}^{(a)}(P) \right\} \left\{ 1 - \frac{P[E_j = 1]}{\bar{P}[E_j = 1]} \right\} \\
&\quad + \mathbb{E}_P \left(E_j \left\{ \frac{1}{\bar{P}[E_j = 1]} - \frac{1}{P[E_j = 1]} \right\} \{ \bar{\mu}_m(a, \mathbf{L}_j) - \mu_m(a, \mathbf{L}_j) \} \right) \\
&\quad + \mathbb{E}_P \left(\frac{E_m}{\bar{P}[E_m = 1]} \left\{ a \frac{\pi_m(\mathbf{L}_m)}{\bar{\pi}_m(\mathbf{L}_m)} + (1-a) \frac{1 - \pi_m(\mathbf{L}_m)}{1 - \bar{\pi}_m(\mathbf{L}_m)} \right\} \{ \bar{\xi}_{j,m}(\mathbf{L}_m) - \xi_{j,m}(\mathbf{L}_m) \} \{ \mu_m(a, \mathbf{L}_m) - \bar{\mu}_m(a, \mathbf{L}_m) \} \right) \\
&\quad + \mathbb{E}_P \left(\frac{E_m}{\bar{P}[E_m = 1]} \left\{ a \left(\frac{\pi_m(\mathbf{L}_m)}{\bar{\pi}_m(\mathbf{L}_m)} - 1 \right) + (1-a) \left(\frac{1 - \pi_m(\mathbf{L}_m)}{1 - \bar{\pi}_m(\mathbf{L}_m)} - 1 \right) \right\} \xi_{j,m}(\mathbf{L}_m) \{ \mu_m(a, \mathbf{L}_m) - \bar{\mu}_m(a, \mathbf{L}_m) \} \right) \\
&\quad + \mathbb{E}_P \left(E_m \left\{ \frac{1}{\bar{P}[E_m = 1]} - \frac{1}{P[E_m = 1]} \right\} \xi_{j,m}(\mathbf{L}_m) \{ \mu_m(a, \mathbf{L}_m) - \bar{\mu}_m(a, \mathbf{L}_m) \} \right) \\
&\quad + \mathbb{E}_P \left(\frac{E_j}{P[E_j = 1]} \{ \bar{\mu}_m(a, \mathbf{L}_j) - \mu_m(a, \mathbf{L}_j) \} - \frac{E_m}{P[E_m = 1]} \xi_{j,m}(\mathbf{L}_m) \{ \bar{\mu}_m(a, \mathbf{L}_m) - \mu_m(a, \mathbf{L}_m) \} \right).
\end{aligned}$$

The result follows as the last two summands simplify:

$$\begin{aligned}
& \mathbb{E}_P \left(\frac{E_m}{P[E_m = 1]} \xi_{j,m}(\mathbf{L}_m) \{ \bar{\mu}_m(a, \mathbf{L}_m) - \mu_m(a, \mathbf{L}_m) \} \right) \\
&= \int_{\mathcal{L}} \frac{p_{\mathbf{L}_j|E_j=1}(\mathbf{l})}{p_{\mathbf{L}_m|E_m=1}(\mathbf{l})} \{ \bar{\mu}_m(a, \mathbf{l}) - \mu_m(a, \mathbf{l}) \} dP_{\mathbf{L}_m|E_m=1}(\mathbf{l}) \\
&= \int_{\mathcal{L}} \{ \bar{\mu}_m(a, \mathbf{l}) - \mu_m(a, \mathbf{l}) \} dP_{\mathbf{L}_j|E_j=1}(\mathbf{l}) \\
&= \mathbb{E}_P (\{ \bar{\mu}_m(a, \mathbf{L}_j) - \mu_m(a, \mathbf{L}_j) \} | E_j = 1) \equiv \mathbb{E}_P \left(\frac{E_j}{P[E_j = 1]} \{ \bar{\mu}_m(a, \mathbf{L}_j) - \mu_m(a, \mathbf{L}_j) \} \right).
\end{aligned}$$

□

Proof of Theorem 3. By the von Mises expansion in Lemma S2 and an application of Lemma 2 of Kennedy et al. (2023), it follows that $\dot{\chi}_{j,m}^{(a)}(O; P)$ is the nonparametric influence function of $\chi_{j,m}^{(a)}$ at P . Given that $\chi_{j,m}(P) = \chi_{j,m}^{(1)}(P) - \chi_{j,m}^{(0)}(P)$ and $\dot{\chi}_{j,m}^*(O; P) = \dot{\chi}_{j,m}^{(1)}(O; P) - \dot{\chi}_{j,m}^{(0)}(O; P)$, this concludes the proof of Theorem 3. □

S1.6 Asymptotic Behavior of $\widehat{\chi}_{j,m}$ (Proof of Theorem 4)

Here we directly analyze the estimator $\widehat{\chi}_{j,m}$; the calculations mirror those for the bias in Lemma S2. Observe that

$$\begin{aligned} & \widehat{\chi}_{j,m} - \chi_{j,m}(P) \\ &= \left\{ \frac{1}{\mathbb{P}_n[E_j]} - \frac{1}{\mathbb{P}[E_j = 1]} \right\} \mathbb{P}_n \left[E_j \{ \widehat{\mu}_m(1, \mathbf{L}_j) - \widehat{\mu}_m(0, \mathbf{L}_j) - \chi_{j,m}(P) \} \right] \\ & \quad + \left\{ \frac{1}{\mathbb{P}_n[E_m]} - \frac{1}{\mathbb{P}[E_m = 1]} \right\} \mathbb{P}_n \left[E_m \widehat{\xi}_{j,m}(\mathbf{L}_m) \left(\frac{A_m}{\widehat{\pi}_m(\mathbf{L}_m)} - \frac{1 - A_m}{1 - \widehat{\pi}_m(\mathbf{L}_m)} \right) (Y_m - \widehat{\mu}_m(A_m, \mathbf{L}_m)) \right] \\ & \quad + \mathbb{P}_n \left[\frac{E_j}{\mathbb{P}[E_j = 1]} \{ \widehat{\mu}_m(1, \mathbf{L}_j) - \widehat{\mu}_m(0, \mathbf{L}_j) - \chi_{j,m}(P) \} \right. \\ & \quad \quad \left. + \frac{E_m}{\mathbb{P}[E_m = 1]} \widehat{\xi}_{j,m}(\mathbf{L}_m) \left(\frac{A_m}{\widehat{\pi}_m(\mathbf{L}_m)} - \frac{1 - A_m}{1 - \widehat{\pi}_m(\mathbf{L}_m)} \right) (Y_m - \widehat{\mu}_m(A_m, \mathbf{L}_m)) \right], \end{aligned}$$

Under our consistency assumptions, and by the central limit theorem (and delta method), the first two summands are $O_P(n^{-1/2}) \times o_P(1) = o_P(n^{-1/2})$. The third summand can be written

$$\begin{aligned} & \mathbb{P}_n [\dot{\chi}_{j,m}^*(O; P)] + \mathbb{P}_n \left[\frac{E_j}{\mathbb{P}[E_j = 1]} \{ \widehat{\mu}_m(1, \mathbf{L}_j) - \widehat{\mu}_m(0, \mathbf{L}_j) - [\mu_m(1, \mathbf{L}_j) - \mu_m(0, \mathbf{L}_j)] \} \right. \\ & \quad \left. + \frac{E_m}{\mathbb{P}[E_m = 1]} \left\{ \widehat{\xi}_{j,m}(\mathbf{L}_m) \left(\frac{A_m}{\widehat{\pi}_m(\mathbf{L}_m)} - \frac{1 - A_m}{1 - \widehat{\pi}_m(\mathbf{L}_m)} \right) (Y_m - \widehat{\mu}_m(A_m, \mathbf{L}_m)) \right. \right. \\ & \quad \quad \left. \left. - \xi_{j,m}(\mathbf{L}_m) \left(\frac{A_m}{\pi_m(\mathbf{L}_m)} - \frac{1 - A_m}{1 - \pi_m(\mathbf{L}_m)} \right) (Y_m - \mu_m(A_m, \mathbf{L}_m)) \right\} \right]. \end{aligned}$$

For the latter term, we can subtract and add the same term but replacing the outer \mathbb{P}_n with \mathbb{E}_P ; the $(\mathbb{P}_n - \mathbb{E}_P)$ contribution is $o_P(n^{-1/2})$ under our assumptions by a simple application of Lemma 2 in Kennedy et al. (2020), while the \mathbb{E}_P contribution is given by

$$\begin{aligned} & \mathbb{E}_P \left(\frac{E_m}{P[E_m = 1]} \frac{\pi_m(\mathbf{L}_m)}{\widehat{\pi}_m(\mathbf{L}_m)} \left\{ \widehat{\xi}_{j,m}(\mathbf{L}_m) - \xi_{j,m}(\mathbf{L}_m) \right\} \{ \mu_m(1, \mathbf{L}_m) - \widehat{\mu}_m(1, \mathbf{L}_m) \} \right) \\ & \quad - \mathbb{E}_P \left(\frac{E_m}{P[E_m = 1]} \frac{1 - \pi_m(\mathbf{L}_m)}{1 - \widehat{\pi}_m(\mathbf{L}_m)} \left\{ \widehat{\xi}_{j,m}(\mathbf{L}_m) - \xi_{j,m}(\mathbf{L}_m) \right\} \{ \mu_m(0, \mathbf{L}_m) - \widehat{\mu}_m(0, \mathbf{L}_m) \} \right) \\ & \quad + \mathbb{E}_P \left(\frac{E_m}{P[E_m = 1]} \left(\frac{\pi_m(\mathbf{L}_m)}{\widehat{\pi}_m(\mathbf{L}_m)} - 1 \right) \xi_{j,m}(\mathbf{L}_m) \{ \mu_m(1, \mathbf{L}_m) - \widehat{\mu}_m(1, \mathbf{L}_m) \} \right) \\ & \quad - \mathbb{E}_P \left(\frac{E_m}{P[E_m = 1]} \left(\frac{1 - \pi_m(\mathbf{L}_m)}{1 - \widehat{\pi}_m(\mathbf{L}_m)} - 1 \right) \xi_{j,m}(\mathbf{L}_m) \{ \mu_m(0, \mathbf{L}_m) - \widehat{\mu}_m(0, \mathbf{L}_m) \} \right), \end{aligned}$$

by the exact same calculations as in the proof of Lemma S2. Again invoking our boundedness assumptions, Theorem 4 follows.

S2 Additional Data Application Details

S2.1 Variable Definitions

Confounders:

- Baseline Age: age at start of target trial

- Sex: {Male, Female}
- Study Site: {KP Washington, KP Northern California, KP Southern California}
- Race: {White, African-American, Other}
- Baseline BMI: BMI value closest to the start of each target trial, up to 1 year prior to the start of target trial
- Self-reported smoking status: Most recent self-reported smoking status prior to the start of the target trial
- Hypertension: Presence of ICD-9 diagnosis code 401.x-405.x up to 1 year prior to start of target trial
- Dyslipidemia: Presence of ICD-9 diagnosis code 272-272.2 or 272.3-272.5, up to 1 year prior to start of target trial
- Type II Diabetes Mellitus: Any of the following:
 - Most recent hemoglobin A1c% $\geq 6.5\%$, up to 2 years prior to the start of target trial
 - Most recent fasting blood glucose ≥ 126 mg/dL, up to 2 years prior to the start of target trial
 - Active prescription for insulin or oral antiglycemic medication (other than Metformin) at the start of the target trial
 - Presence of ICD-9 diagnosis code 250.x within 1 year prior to start of target trial and active prescription for Metformin at start of target trial.
- Medications
 - Insulin: active prescription for insulin at the start of the target trial
 - Antihypertensives: active prescription for antihypertensive medication at the start of the target trial
 - Antilipemic: active prescription for antilipemic medication at the start of the target trial

Outcomes:

Let BMI_m denote baseline BMI at trial m . Relative weight changes since baseline ($t = 0$) and at some follow-up time t (e.g., one of 6 months, 1 year, 2 years, 3 years) were computed as

$$Y_m = \frac{BMI_{m+t} - BMI_m}{BMI_m}$$

where BMI_{m+t} was ascertained using the window method of [Thaweethai et al. \(2021\)](#). To compute BMI at 3-years, for example, the following procedures was used:

1. Let $Date_{m+36}$ denote the date exactly 3 years after the the start of target trial m .
2. Consider a window ± 6 months around $Date_{m+36}$, $[Date_{m+30}, Date_{m+42}]$
3. If a patient has BMI measures in both $[Date_{m+30}, Date_{m+36})$ and $(Date_{m+36}, Date_{m+42}]$, fit a linear regression to all BMI measures $[Date_{m+30}, Date_{m+42}]$ and take BMI_{m+36} to be the interpolated (e.g., fitted) value at $t = 36$ months.

4. If a patient only has BMI measures in $[\text{Date}_{m+30}, \text{Date}_{m+36})$ or $(\text{Date}_{m+36}, \text{Date}_{m+42}]$ but not both, take BMI_{m+36} to be the measure recorded closest to Date_{m+36} .
5. If a patient had no BMI measures in $[\text{Date}_{m+30}, \text{Date}_{m+42}]$, take BMI_{m+36} to be missing.

Practically, we exclude patients with missing outcomes by setting $E_m = 0$ if $Y_m = \text{NA}$. We leave more comprehensive treatment of missing outcomes within our framework as an extension for future work.

Outcomes for additional time points were computed in a similar manner using the following window lengths:

1. BMI at 6 Months (± 2 month window)
2. BMI at 1 Year (± 3 month window)
3. BMI at 2 Years (± 6 month window)

S2.2 Analytic Methods

All pooled models were estimated using random forests (`ranger`) (Wright and Ziegler, 2017). We opted for `ranger` rather than `SuperLearner` (Polley et al., 2023) (as in simulations) due to computational speed in light of the size of pooled data \mathcal{D} . In particular, the following configurations were used.

- Outcome Model $\tilde{\mu}$ (stratified by treatment status):
 - `num.trees` = 500
 - `max.depth` = 10
- Treatment Model $\tilde{\pi}$:
 - `num.trees` = 500
 - `max.depth` = 2
- Transport Model $\tilde{\xi}$:
 - `num.trees` = 500
 - `max.depth` = 10

Inverse probability of treatment weights were truncated (Hernán and Robins, 2024) at the 99% quantile within each treatment arm. Similarly, ratios $\frac{P(T=j | \mathbf{L}, E=1)}{P(T=m | \mathbf{L}, E=1)}$ were also truncated at the 99% quantile across all (j, m) pairs.

Candidate marginal structural models for projection models were as follows:

- Constant $\psi_m(m; \boldsymbol{\beta}) = \beta$
- Linear $\psi_m(m; \boldsymbol{\beta}) = \beta_0 + \beta_1 m$
- Cubic $\psi_m(m; \boldsymbol{\beta}) = \beta_0 + \beta_1 m + \beta_2 m^2 + \beta_3 m^3$
- Spline (2 knots)
 - Knots at $m \in \{24, 48\}$ for Surgery versus No Surgery and RYGB versus No Surgery

- Knots at $m \in \{48, 72\}$ for SG versus No Surgery and RYGB versus SG
- Spline (3 knots)
 - Knots at $m \in \{12, 36, 60\}$ for Surgery versus No Surgery and RYGB versus No Surgery
 - Knots at $m \in \{40, 56, 72\}$ for SG versus No Surgery and RYGB versus SG

S2.3 Additional Application Figures and Tables

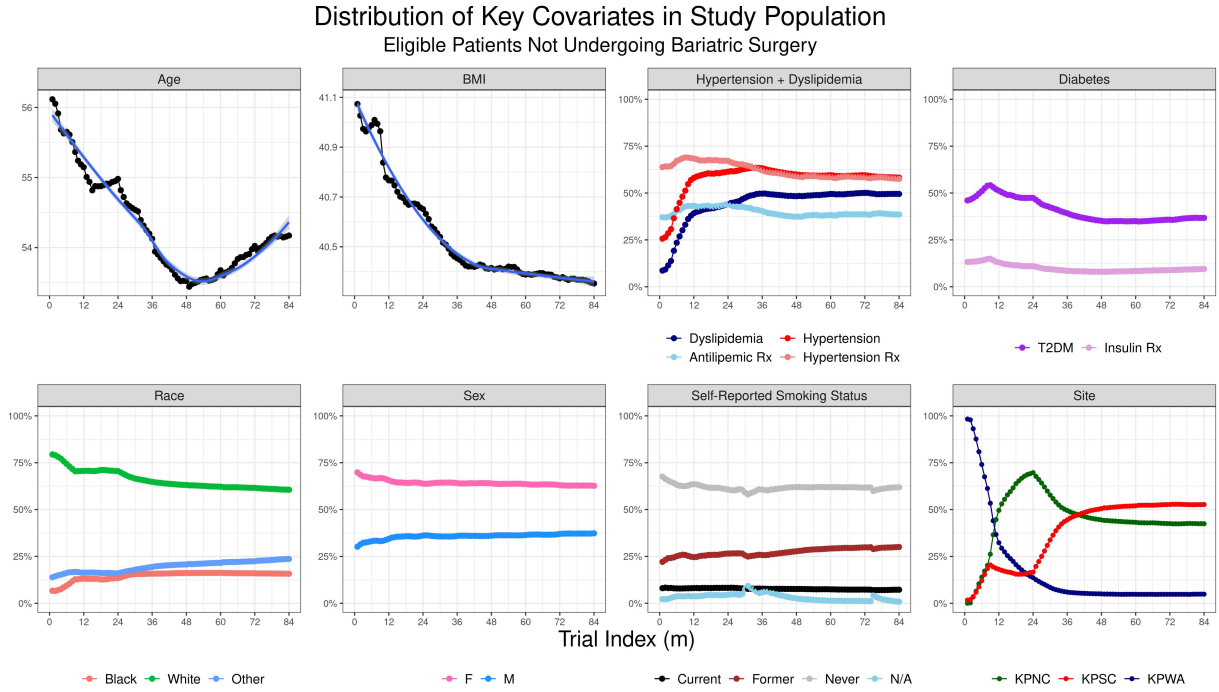


Figure S1: Distribution of patient characteristics in DURABLE electronic health record database over calendar time for eligible patients not undergoing bariatric surgery between 2005-2011. Covariate mean values (continuous covariates) or frequency (binary/categorical covariates) are plotted by month of surgery. $m = 1$ corresponds to January 2005 and $m = 84$ corresponds to December 2011.

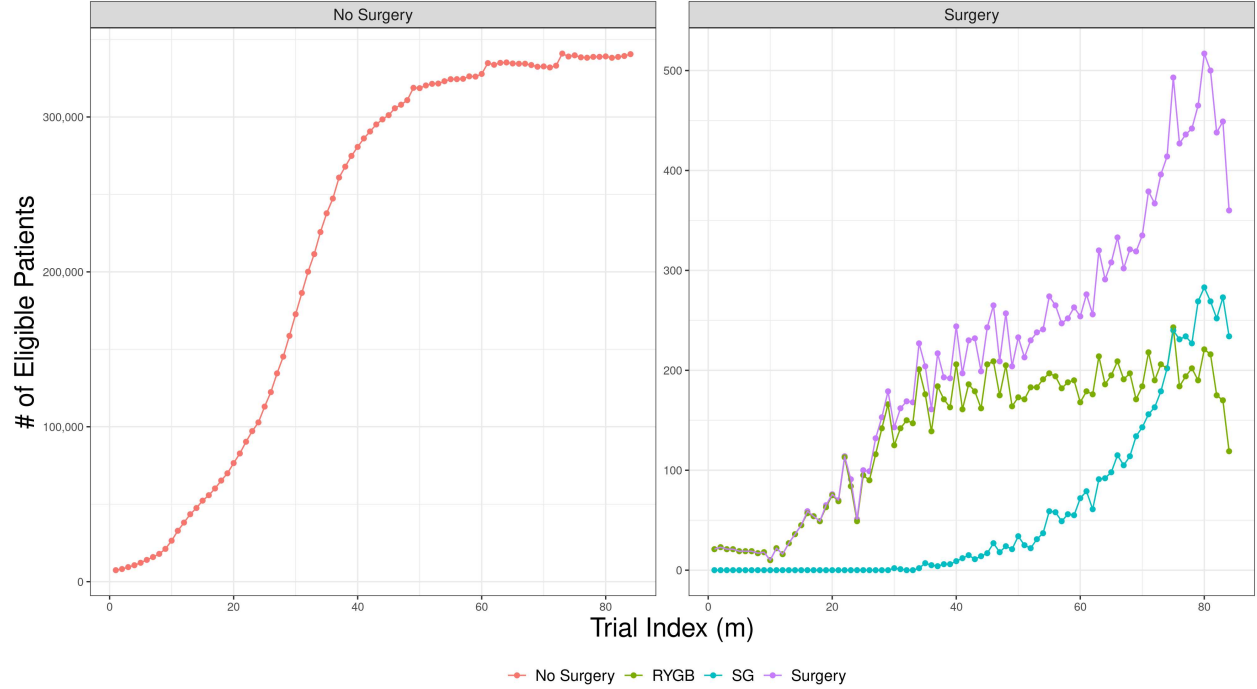


Figure S2: Number of patients meeting eligibility criteria in each target trial, by treatment status. Note that in addition to RYGB and SG procedures, the surgery group includes a small number of adjustable gastric banding procedures.

Comparison	Outcome	Constant	Linear	Cubic	Spline (2 Knots)	Spline (3 Knots)
Surgery vs. No Surgery	6 Months	-3.518 (12.91)	-3.525 (3.47)	-3.527 (0.01)	-3.527 (0.36)	-3.527 (0.00)
	1 Year	-5.251 (23.79)	-5.267 (6.97)	-5.273 (0.37)	-5.273 (0.61)	-5.274 (0.00)
	2 Years	-4.552 (26.05)	-4.573 (4.55)	-4.577 (0.38)	-4.577 (0.00)	-4.576 (0.98)
	3 Years	-3.625 (44.40)	-3.659 (16.01)	-3.675 (2.04)	-3.675 (1.99)	-3.678 (0.00)
RYGB vs. No Surgery	6 Months	-4.222 (1.81)	-4.223 (0.78)	-4.223 (0.00)	-4.223 (0.14)	-4.223 (0.13)
	1 Year	-6.474 (4.71)	-6.476 (3.10)	-6.478 (0.75)	-6.479 (0.32)	-6.479 (0.00)
	2 Years	-5.791 (7.84)	-5.792 (6.60)	-5.794 (5.32)	-5.796 (3.87)	-5.800 (0.00)
	3 Years	-4.645 (10.70)	-4.647 (8.71)	-4.655 (3.14)	-4.656 (2.07)	-4.659 (0.00)
SG vs. No Surgery	6 Months	-1.813 (0.42)	-1.813 (0.56)	-1.814 (0.30)	-1.814 (0.29)	-1.814 (0.00)
	1 Year	-2.490 (0.00)	-2.486 (6.16)	-2.486 (5.88)	-2.486 (6.08)	-2.486 (5.39)
	2 Years	-2.020 (0.01)	-2.020 (0.00)	-2.020 (0.41)	-2.020 (0.37)	-2.020 (0.05)
	3 Years	-1.466 (0.00)	-1.463 (3.58)	-1.464 (2.41)	-1.464 (2.57)	-1.465 (1.92)
RYGB vs. SG	6 Months	-0.101 (0.47)	-0.101 (0.27)	-0.101 (0.08)	-0.101 (0.09)	-0.102 (0.00)
	1 Year	-0.220 (0.00)	-0.217 (2.75)	-0.217 (2.87)	-0.217 (2.71)	-0.217 (2.53)
	2 Years	-0.288 (0.00)	-0.283 (3.73)	-0.281 (6.00)	-0.281 (6.08)	-0.281 (5.87)
	3 Years	-0.298 (0.00)	-0.297 (1.00)	-0.296 (1.87)	-0.296 (1.85)	-0.297 (1.16)

Table S1: Values of loss function $L(\hat{\psi}_k)$ for each candidate MSM. Cells in bold denote the MSM $\hat{\psi}^*$ which minimizes $L(\hat{\psi}_k)$ in each setting. Values in parenthesis denote the number of weighted standard deviations, ϵ , by which $L(\hat{\psi}_k)$ exceeds $L(\hat{\psi}^*)$.

S3 Simulations

S3.1 Simulation Overview

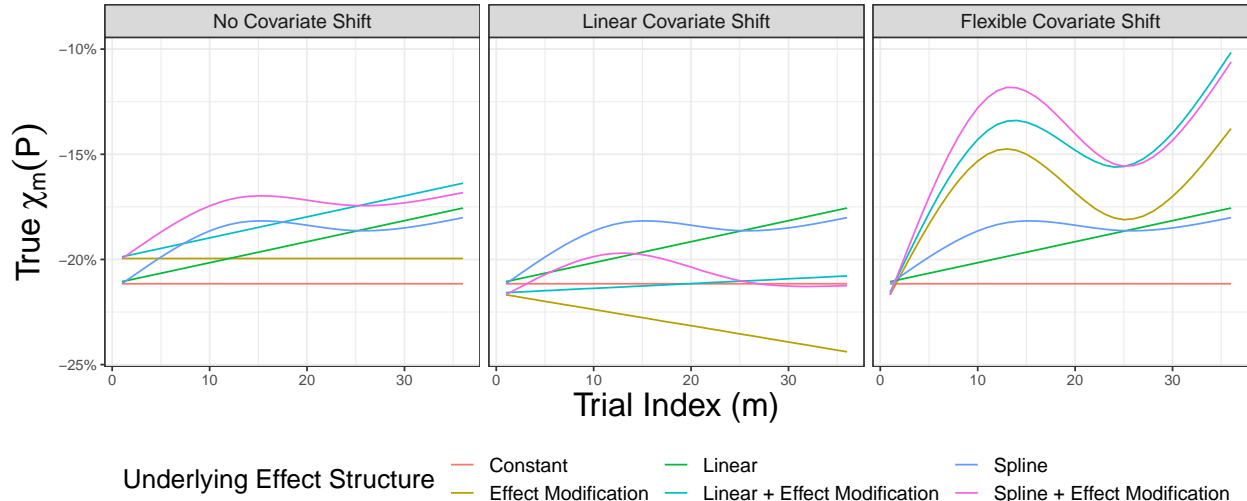


Figure S3: Overview of calendar time-specific treatment effects across simulation scenarios.

To evaluate the practical utility and assess the finite-sample properties of the proposed methods, we conducted an extensive plasmode simulation study (Vaughan et al., 2009) closely linked to the EHR data underlying our bariatric surgery analysis. Our setup considered $M = 36$ target trials assessing the effect of a binary treatment A on a continuous outcome Y , using observed covariates \mathbf{L} from DURABLE (sex, age, BMI, study site, race, smoking status, hypertension, dyslipidemia, diabetes, medication usage). To maintain direct control over the structure of covariate shift across trials, we conceptualize A as a treatment whose receipt does not exclude patients from future trials. In the simulated setup, exclusion of such patients would lead to a depletion of eligible patients in later trials, thus indirectly changing the distribution of covariates among the eligible population, and complicating the ability to analytically control the structure of simulated effects across calendar time. As detailed below, we used models based on $A \in \{\text{surgery, no surgery}\}$ and $Y = 3\text{-year relative weight change}$ to inform the strength of associations between \mathbf{L} , A and Y in our simulation study.

To generate simulated datasets, we first sampled entire covariate vectors \mathbf{L}_1 from the observed distribution in the DURABLE data, in order to preserve the complex correlation structure typical of EHR data. Covariate vectors for the remaining trials $m \in \{2, \dots, M\}$ were generated under one of three settings. First, we considered no covariate shift, which we enforced by setting $\mathbf{L}_m = \mathbf{L}_1$ for $m \in \{2, \dots, M\}$. Second, we considered a linear covariate shift by allowing both the prevalence of diabetes and mean BMI to vary linearly across trials, while age naturally increased linearly as well. Finally, we considered a form of flexible covariate shift such that the prevalence of diabetes and mean BMI followed splines on m (along with linear increase in age).

Simulated treatments and outcomes were generated using covariates \mathbf{L}_m and logistic/linear regression models, respectively, tied closely to our bariatric surgery example. Coefficient values for these models were informed by fits of pooled logistic regression ($\tilde{\pi}$) and linear outcome models ($\tilde{\mu}$) estimated from 14,353,682 subject-trials in the DURABLE database. Simulated outcomes were generated following one of six distinct outcome models, each encoding different interaction structures among A_m , m , and \mathbf{L}_m , and thus representing different patterns of treatment effect variation over calendar time. The six treatment effect structures were as follows: (1) Constant (A); (2) linear

($A \times m$); (3) spline ($A \times f(m)$ for spline basis $f(m)$), (4) effect modification ($A \times \mathbf{L}_m$); (5) linear + effect modification ($A \times m + A \times \mathbf{L}_m$); and (6) spline + effect modification ($A \times f(m) + A \times \mathbf{L}_m$). Interactions of the form $A \times \mathbf{L}_m$ were specified for age, BMI, and diabetes status, the covariates subject to controlled shifts across trials, thereby inducing change in trial-specific treatment effects independent of patterns in underlying treatment efficacy.

Together, the three forms of covariate shift and six outcome model structures comprise 18 distinct simulation scenarios. Figure S3 summarizes the true values of $\chi_m(P)$ over time for each scenario. Additional details on data generation in each scenario is provided in Section S3.2, while complete tables of coefficients used to generate simulated data are provided in Section S3.5. For each scenario, 1,000 simulated datasets were generated for sample sizes $n \in \{100, 500, 1000, 5000, 10000, 25000\}$. Although these total unique patient numbers are smaller than in our motivating application (to reduce computational burden), the resulting pooled datasets still contain nearly 1,000,000 subject-trials when $n = 25,000$, consistent with the scale of EHR-based studies of bariatric surgery (Benz et al., 2024, Haneuse et al., 2025).

S3.2 Simulation Data Generating Process

Simulated data were according to the following steps. In the below steps, we let $\boldsymbol{\alpha}_f$ and \mathbf{X}_f respectively denote the coefficient vector and design matrix relevant to nuisance function $f(\cdot)$. Specific values for $\boldsymbol{\alpha}_f$ are presented in Section S3.5.

1. Draw \mathbf{L}_1 from observed eligible subject-trials in the DURABLE database.
2. Update covariates ($\mathbf{L}_2, \dots, \mathbf{L}_M$) according to one of the three rules described in more detail below.
3. Sample treatment $A \mid \mathbf{L}_m \sim \text{Bernoulli}(\pi_m(\mathbf{L}_m))$ where $\text{logit}[\pi_m(\mathbf{L}_m)] = \boldsymbol{\alpha}_\pi^T \mathbf{X}_\pi$
4. Sample outcome $Y_m \mid \mathbf{L}_m, A_m \sim \mathcal{N}(\mu_m(A_m, \mathbf{L}_m), \sigma_y^2)$ where $\mu_m(A_m, \mathbf{L}_m) = \boldsymbol{\alpha}_\mu^T \mathbf{X}_\mu$. Note that μ_m takes one of 6 forms described in more details below.

Covariate Shift Rules:

Covariate shift across component trials followed one of three update rules.

1. No covariate shift: $\mathbf{L}_m = \mathbf{L}_1$ for all m
2. Linear covariate shift:
 - (a) $\text{BMI}_m = \text{BMI}_1 + \mathcal{N}\left(\frac{m-1}{12}, 1\right)$
 - (b) $P(\text{Diabetes}_m = 1) = 0.2 + \frac{0.4(m-1)}{35}$
 - (c) $\text{Age}_m = \text{Age}_1 + \frac{m-1}{12}$
 - (d) No change in remaining covariates
3. Flexible covariate shift
 - (a) $\text{BMI}_m = \text{BMI}_1 + \mathcal{N}\left(\mathbf{x}_m^T(1, -3, 1), 1\right)$
 - (b) $P(\text{Diabetes}_m = 1) = 0.2 + \mathbf{x}_m^T(0.02, 0.6, -0.08)$
 - (c) $\text{Age}_m = \text{Age}_1 + \frac{m-1}{12}$
 - (d) No change in remaining covariates

Note that the update rules for diabetes ensure that the prevalence varies between 20% at $m = 1$ to 60% at $m = 36$. In the above \mathbf{x}_m^T , denotes the m^{th} row of the spline design matrix that is the result of a natural cubic spline on $\{1, \dots, 36\}$ with 2 internal knots, `ns(1:36, df = 3)`.

Outcome Models:

Generation of outcomes Y_m followed one of six different outcome models, each encoding a treatment effect structure with different reasons how and why treatment effects vary by calendar time. In the below, we use the shorthand $A_m \times \mathbf{L}_m$ to denote treatment-confounder interactions. Specific interactions are with age, BMI, and diabetes status. Effect structures across calendar time are as follows. As before, \mathbf{x}_m denotes the m^{th} row of the design matrix resulting from a natural cubic spline on $\{1, \dots, 36\}$ with 2 internal knots, `ns(1:36, df = 3)`.

1. Constant: $\mathbb{E}[Y_m \mid \mathbf{A}_m, \mathbf{L}_m] = \alpha_0 + \boldsymbol{\alpha}_1 \mathbf{L}_m + \alpha_2 A_m$
2. Linear: $\mathbb{E}[Y_m \mid \mathbf{A}_m, \mathbf{L}_m] = \alpha_0 + \boldsymbol{\alpha}_1^T \mathbf{L}_m + \alpha_2 A_m + \alpha_3 (A_m \times m)$
3. Spline: $\mathbb{E}[Y_m \mid \mathbf{A}_m, \mathbf{L}_m] = \alpha_0 + \boldsymbol{\alpha}_1^T \mathbf{L}_m + \alpha_2 A_m + \boldsymbol{\alpha}_3^T (A_m \times \mathbf{x}_m)$
4. Effect Modification: $\mathbb{E}[Y_m \mid \mathbf{A}_m, \mathbf{L}_m] = \alpha_0 + \boldsymbol{\alpha}_1^T \mathbf{L}_m + \alpha_2 A_m + \boldsymbol{\alpha}_3^T (A_m \times \mathbf{L}_m)$
5. Linear + Effect Modification: $\mathbb{E}[Y_m \mid \mathbf{A}_m, \mathbf{L}_m] = \alpha_0 + \boldsymbol{\alpha}_1^T \mathbf{L}_m + \alpha_2 A_m + \alpha_3 (A_m \times m) + \boldsymbol{\alpha}_4^T (A_m \times \mathbf{L}_m)$
6. Spline + Effect Modification: $\mathbb{E}[Y_m \mid \mathbf{A}_m, \mathbf{L}_m] = \alpha_0 + \boldsymbol{\alpha}_1^T \mathbf{L}_m + \alpha_2 A_m + \boldsymbol{\alpha}_3^T (A_m \times \mathbf{x}_m) + \boldsymbol{\alpha}_4^T (A_m \times \mathbf{L}_m)$

S3.3 Analysis Methods

To estimate $\hat{\chi}_m$, we used `SuperLearner` (Polley et al., 2023) for pooled outcome and propensity models. Pooled outcomes models were estimated separately for each treatment status. Component libraries included (generalized) linear models (`SL.speedglm`), generalized additive models (`SL.gam`) and random forests (`SL.ranger`). Because the `SuperLearner` package does not provide support for categorical outcomes, we used a random forest model for ξ when estimating cross-trial effects. We considered five candidate MSMs for projection: (1) constant model, (2) linear model, (3) cubic model, (4) spline with 2 knots at $m \in \{12, 24\}$, and (5) spline with 3 knots at $m \in \{9, 18, 27\}$.

Pooled Models

- Outcome Model $\tilde{\mu}$ used `SuperLearner`, stratified by treatment status, with the following component libraries
 - `SL.speedglm`
 - `SL.gam` with `deg.gam = 4`
 - `SL.ranger` with `max.depth = 10` and `num.trees = 500`
- Treatment Model $\tilde{\pi}$ used `SuperLearner` with the following component libraries
 - `SL.speedglm`
 - `SL.gam` with `deg.gam = 4`
 - `SL.ranger` with `max.depth = 4` and `num.trees = 500`

- Transport Model $\tilde{\xi}$ used random forest (`ranger`) with `max.depth = 10` and `num.trees = 500`

Correction of $\hat{\theta}_m$ in Complete Absence of Effect Modification:

In simulation settings where the true treatment effect is constant over calendar time, even with covariate shift (i.e., there is no effect modification) differences between $\hat{\chi}_{j,m_1}$ and $\hat{\chi}_{j,m_2}$ can be effectively 0. However, if because there is no effect modification detected by nuisance models (if consistent), any sampling variation in outcome differences is attributed to changes in the calendar time index, thus producing estimates $\hat{\theta}_m$ closer to 1. If differences between $\hat{\chi}_{j,m_1}$ and $\hat{\chi}_{j,m_2}$ are indeed extremely small, this undesirable behavior given that we'd like values of $\theta \approx 1$ to reflect possible shifts in treatment efficacy. Further more, this is somewhat of an artifact of our simulation set up given that scenarios without any covariate shift and/or effect modification are not reflective of EHR-based target trial emulations. To “correct” this behavior in our simulations, we apply a data-adaptive thresholding procedure, as follows.

1. Compute $\hat{\sigma}_m = \frac{1}{M-1} \sum_{j=1}^M (\hat{\chi}_m - \hat{\chi}_{m,j})^2$, $\hat{\gamma}_m = \frac{1}{M-1} \sum_{j=1}^M (\hat{\chi}_m - \hat{\chi}_{j,m})^2$ as usual.
2. Compute $\hat{\sigma}_m^{\prime 2} = \frac{1}{M-1} \sum_{j=1}^M t(\hat{\chi}_m - \hat{\chi}_{m,j}, 0.005)^2$, $\hat{\gamma}_m^{\prime} = \frac{1}{M-1} \sum_{j=1}^M t(\hat{\chi}_m - \hat{\chi}_{j,m}, 0.005)^2$, where $t(x, d) = \mathbb{1}(|x| > d)|x|$
3. Compute $\hat{\theta}_m$ as follows

$$\hat{\theta}_m = \begin{cases} \frac{\hat{\sigma}_m^2}{\hat{\sigma}_m^2 + \hat{\gamma}_m^2} & \left| \frac{\hat{\sigma}_m^2}{\hat{\sigma}_m^2 + \hat{\gamma}_m^2} - \frac{\hat{\sigma}_m^{\prime 2}}{\hat{\sigma}_m^{\prime 2} + \hat{\gamma}_m^{\prime}} \right| \leq 0.1 \\ \frac{\hat{\sigma}_m^{\prime 2}}{\hat{\sigma}_m^{\prime 2} + \hat{\gamma}_m^{\prime}} & \left| \frac{\hat{\sigma}_m^2}{\hat{\sigma}_m^2 + \hat{\gamma}_m^2} - \frac{\hat{\sigma}_m^{\prime 2}}{\hat{\sigma}_m^{\prime 2} + \hat{\gamma}_m^{\prime}} \right| > 0.1 \end{cases}$$

The above procedure replaces $\hat{\theta}_m$ by a thresholded version if and only if replacing differences smaller than 0.005 changes the variability ratio by more than 10% (absolutely). The only circumstances which would lead to replacement a thresholded version of $\hat{\theta}_m$ are which all of the variability in cross trial effects are explained by differences smaller than 0.005. Given the magnitude of treatment effect changes across time in our simulation setting (Figure 3), this is only possible if the underlying treatment effect structure is constant.

S3.4 Simulation Results

Key simulation results are presented in Figure S4. Figure S4A shows the frequency with which each candidate MSM was selected across 1,000 simulations for varying values of $c \in \{0, 0.25, 0.5, 0.75, 1\}$. Simply selecting the MSM minimizing $\hat{L}(\hat{\psi}_k)$ without any form of penalization ($c = 0$) often resulted in selection of the most flexible MSM, even when the true underlying effect structure was constant across time. As c increased, so too did the sample size required for selection of more complex MSMs, even in cases where the more complex model was the correct underlying data generating mechanism. A good example of this is illustrated by the outcome model with a linear treatment effect and effect modification under linear covariate shift. As seen in Figure S3, the induced trend in calendar time is linear in m with a very shallow slope. A sample size of $n = 25,000$ was required to preferentially select the linear MSM with $c = 0.25$, while the constant model remained the most common selection for larger values of c . Similar behavior was observed for scenarios where the induced trend across calendar time followed a spline. Using $c = 0.25$, the correct MSM was the majority selection across all scenarios.

True values of θ_m are plotted in the rightmost column of Figure S4B. The remaining columns of Figure S4B present mean values of $\hat{\theta}_m = \frac{\hat{\sigma}_m^2}{\hat{\sigma}_m^2 + \hat{\gamma}_m^2}$ across simulations. In scenarios where the underlying treatment effect structure does not contain interactions with m (e.g., constant, effect modification),

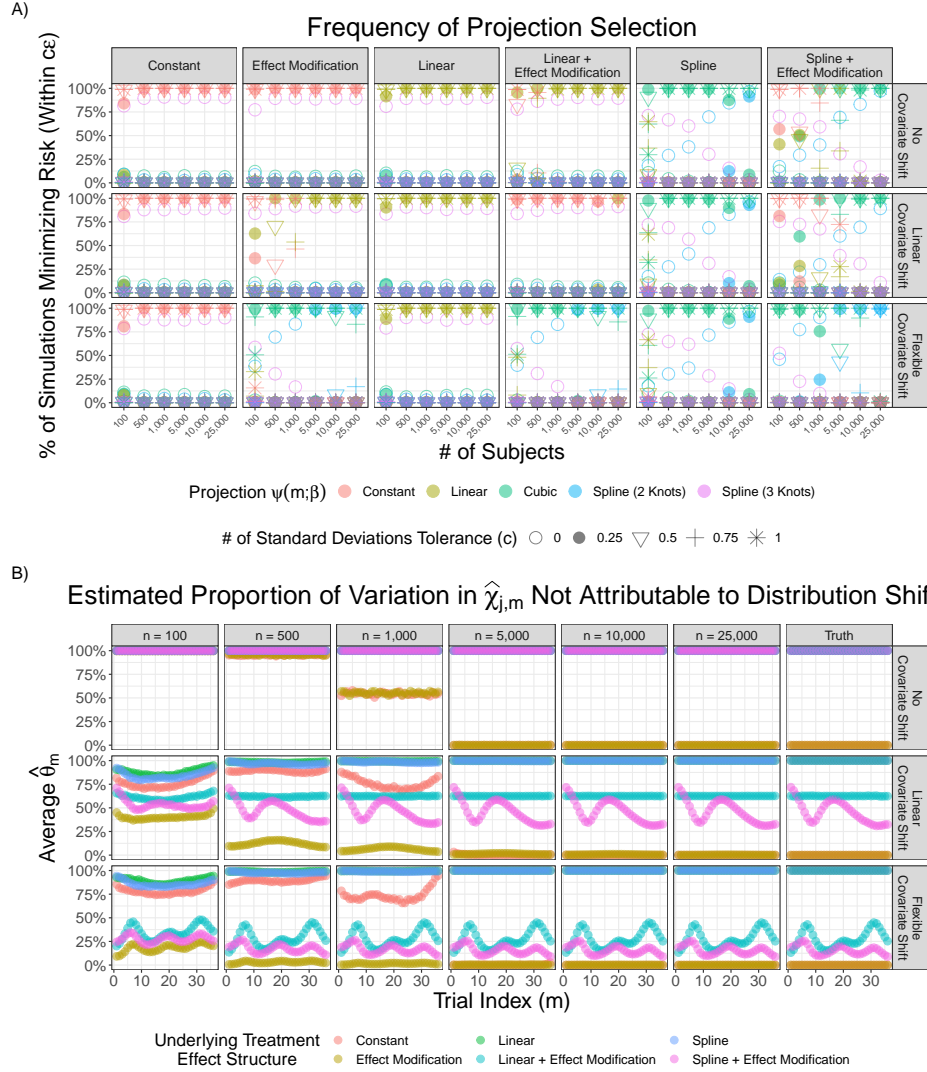


Figure S4: (A) Proportion of simulations in which each of five candidate MSMs was selected as the model minimizing $\hat{L}(\hat{\psi}_k)$. Results are shown for various values of $c \in \{0, 0.25, 0.5, 0.75, 1\}$. (B) Average values of trial-specific variability ratios, $\hat{\theta}_m$, across varying sample sizes.

$\theta_m = 0$ across time. Conversely, in scenarios with linear or spline based effect structures, $\theta_m = 1$ for all m . When changes in effects are attributable to both changes in treatment efficacy and covariate shift in effect modifiers, $\theta_m \in (0, 1)$ and varies across time.

Across scenarios, $\hat{\theta}_m$ was unbiased for θ_m beyond $n = 5,000$ subjects. The greatest degree of bias was observed in smaller samples for scenarios where $\theta = 0$. In scenarios with a constant treatment effect, note that both σ_m^2 and $\gamma_m^2 \approx 0$, and thus extremely small differences in estimated time-specific ATEs can produce biased estimates of θ closer to 1. This issue underscores the importance of simultaneously considering the selected MSM, as in all of these cases, a constant model is most frequently selected (Figure S4A).

Figure S5 shows hypothesis testing results from our simulation study. The y-axis of Figure S5 displays the proportion of simulations for which the correct decision is made, that is rejecting H_0 when H_1 is true, and failing to reject H_0 when H_0 is true. For scenarios in which the true θ is not at a boundary point, this is power. For scenarios at a boundary point, this is specificity. Unfortunately,

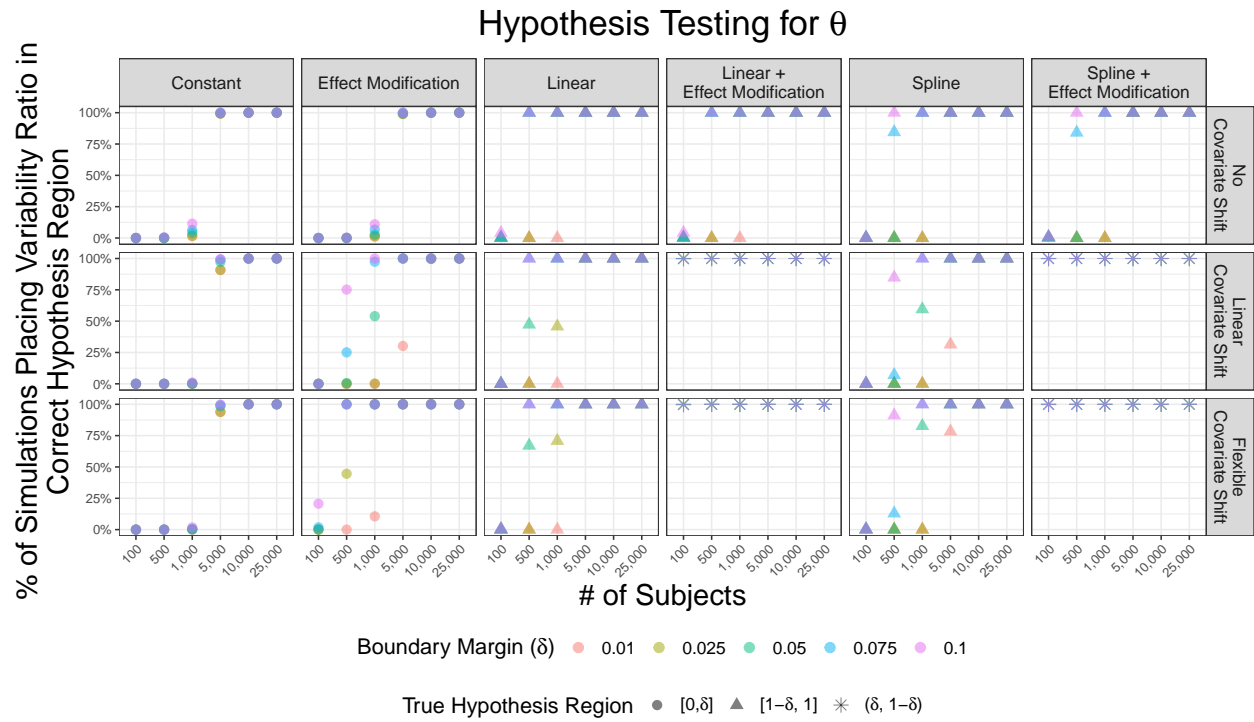


Figure S5: Results from hypothesis testing across simulations

it is not directly possible to show type I error rate, as type 1 error is preserved at the nominal level only the boundary margin, δ , yet the true value $\theta \neq \delta$. In general, for larger sample sizes, there is very good power to reject H_0 when θ is not at a boundary point and good specificity when θ is at a boundary point.

S3.5 Simulation Parameters

Term	π_m	μ_m					
		1	2	3	4	5	6
(Intercept)	-2.49	9.8×10^{-2}					
baseline_bmi	6.7×10^{-2}	-1.9×10^{-3}					
gender	-1.01	4.7×10^{-3}					
race	0.41	-3.1×10^{-3}					
site[NC]	-0.39	-2.4×10^{-3}					
site[SC]	0.35	-7.9×10^{-3}					
baseline_age	-4.9×10^{-2}	-6.1×10^{-4}					
t2dm	-3.4×10^{-2}	-1.2×10^{-2}					
insulin	-2×10^{-2}	1.3×10^{-2}	1.3×10^{-2}	1.3×10^{-2}	1.3×10^{-2}	1.3×10^{-2}	1.3×10^{-2}
hypertension	0.70	1.3×10^{-3}					
hypertension_rx	-0.34	-8×10^{-5}					
dyslipidemia	0.42	-8.8×10^{-4}					
antilipemic_rx	-0.21	3.6×10^{-4}					
smoking_status[former]	2.16	-2.6×10^{-3}					
smoking_status[never]	1.66	4.6×10^{-4}					
treatment	—	-0.21	-0.21	-0.21	0.67	0.67	0.67
trial_id:treatment	—	—	1×10^{-3}	—	—	1×10^{-3}	—
treatment:spline_1	—	—	—	1×10^{-2}	—	—	1×10^{-2}
treatment:spline_2	—	—	—	6×10^{-2}	—	—	6×10^{-2}
treatment:spline_3	—	—	—	1×10^{-2}	—	—	1×10^{-2}
baseline_age:treatment	—	—	—	—	2×10^{-3}	2×10^{-3}	2×10^{-3}
t2dm:treatment	—	—	—	—	1×10^{-1}	1×10^{-1}	1×10^{-1}
baseline_bmi:treatment	—	—	—	—	-2.5×10^{-2}	-2.5×10^{-2}	-2.5×10^{-2}

Table S2: Summary of coefficients used for simulated treatments A_m (from π_m) and outcomes Y_m (from μ_m). Outcome model numbering reflects the ordering of scenarios described in Section S3.2.

References

- Luke Benz, Rajarshi Mukherjee, Rui Wang, David Arterburn, Heidi Fischer, Catherine Lee, Susan M Shortreed, and Sebastien Haneuse. Adjusting for selection bias due to missing eligibility criteria in emulated target trials. *American Journal of Epidemiology*, page kwae471, 2024.
- Peter J. Bickel, Chris A. J. Klaassen, and Jon A. Wellner. *Efficient and Adaptive Estimation for Semiparametric Models*, volume 4. Johns Hopkins University Press, Baltimore, 1993.
- Sebatien Haneuse, Luke Benz, Valerie A. Smith, David Arterburn, and Matthew L. Maciejewski. Long-term cardiovascular outcomes following bariatric surgery: Reconciling seemingly conflicting evidence. *Epidemiology*, 2025. In press.
- MA Hernán and J Robins. *Causal Inference: What if*. Boca Raton: Chapman & Hall/CRC, 2024.
- Edward H Kennedy, Sivaraman Balakrishnan, and Max G’Sell. Sharp instruments for classifying compliers and generalizing causal effects. *The Annals of Statistics*, 48(4):2008–2030, 2020.
- Edward H Kennedy, Sivaraman Balakrishnan, and Larry A Wasserman. Semiparametric counterfactual density estimation. *Biometrika*, 110(4):875–896, 2023. doi: 10.1093/biomet/asad017.
- Eric Polley, Erin LeDell, Chris Kennedy, and Mark van der Laan. Superlearner: Super learner prediction. <https://CRAN.R-project.org/package=SuperLearner>, 2023. R package version 2.0-28.1.
- Tanayott Thaweethai, David E. Arterburn, Karen J. Coleman, and Sebastien Haneuse. Robust inference when combining inverse-probability weighting and multiple imputation to address missing data with application to an electronic health records-based study of bariatric surgery. *Ann. Appl. Stat.*, 15(1):126–147, 2021. doi: 10.1214/20-AOAS1386.
- Aad W. van der Vaart and Jon A. Wellner. *Weak Convergence and Empirical Processes: With Applications to Statistics*. Springer Series in Statistics. Springer, New York, 1st edition, 1996.
- AW van der Vaart. Semiparametric statistics. In *Lectures on probability theory and statistics (Saint-Flour, 1999)*, pages 331–457. Springer, 2002.
- Laura K. Vaughan, Jasmin Divers, Miguel A. Padilla, D. Ted Redden, Hemant K. Tiwari, Daniel Pomp, et al. The use of plasmodes as a supplement to simulations: a simple example evaluating individual admixture estimation methodologies. *Computational Statistics & Data Analysis*, 53(5): 1755–1766, 2009. doi: 10.1016/j.csda.2008.02.016.
- Marvin N. Wright and Andreas Ziegler. ranger: A fast implementation of random forests for high dimensional data in C++ and R. *Journal of Statistical Software*, 77(1):1–17, 2017. doi: 10.18637/jss.v077.i01.